

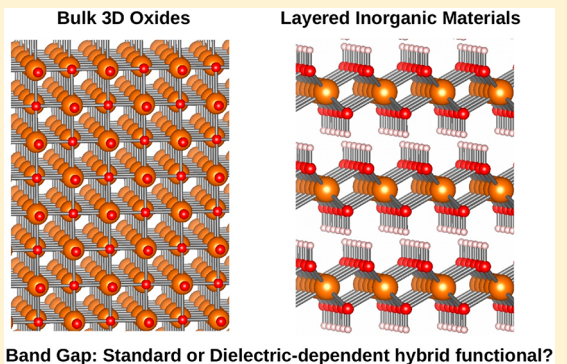
Band Gap of 3D Metal Oxides and Quasi-2D Materials from Hybrid Density Functional Theory: Are Dielectric-Dependent Functionals Superior?

Tilak Das, Giovanni Di Liberto,^{ip} Sergio Tosoni,^{ip} and Gianfranco Pacchioni^{*ip}

Dipartimento di Scienza dei Materiali, Università di Milano—Bicocca, via R. Cozzi 55, 20125 Milano, Italy

Supporting Information

ABSTRACT: Reproduction of the band gaps of semiconductors and insulators represents a well-known problem for standard DFT approaches based on semilocal functionals. The problem can be partly solved using hybrid functionals, in which a given portion of exact exchange is mixed with the DFT exchange. Recently, a new class of dielectric-dependent functionals has been introduced in which the amount of exact exchange is derived from the static dielectric function of a given compound. In this study we considered in a systematic way on an equal footing a set of 24 nonmagnetic three-dimensional (3D) bulk metal oxides and 24 quasi-two-dimensional (quasi-2D) semiconductors (oxides, hydroxides, chlorides, oxyhalides, nitrides, and transition metal dichalcogenides) and computed the corresponding Kohn–Sham band gaps with three global hybrid functionals and four range-separated hybrid functionals. These in turn were divided into standard (PBE0, B3LYP, HSE06, SC-BLYP) and dielectric-dependent (DD-B3LYP, DD-SC-BLYP, DD-CAM-B3LYP) functionals. We also performed a statistical analysis of the DFT data set along with structural parameters of these 2D and 3D materials. The surprising result is that overall there is no real improvement with the use of dielectric-dependent functionals compared to PBE0, HSE06, and B3LYP. Short-range DD-SC-BLYP gives a minor improvement in the band gaps for bulk metal oxides compared with standard SC-BLYP, but the mean absolute error is still 0.12 eV higher than with B3LYP. The use of dielectric-dependent standard or short-range functionals such as DD-B3LYP or DD-HSE06 worsens the situation. However, the dielectric-dependent version of the long-range-separated functional implemented with the Coulomb attenuating method (CAM), DD-CAM-B3LYP, leads to a clear improvement for band gaps of quasi-2D materials. On the basis of this analysis, the conclusion is that the use of a standard hybrid functional such as B3LYP or HSE06 is recommended for nonmagnetic bulk 3D metal oxides. On the other hand, the treatment of layered materials such as MoO₃ or V₂O₅ benefits from the use of dielectric-dependent range-separated functionals.



1. INTRODUCTION

The problem of describing the Kohn–Sham (KS) band gap in materials with insulating and semiconducting character is well-known in the solid-state physics and chemistry communities. On the experimental side, the information on band gaps can be obtained with different techniques, either measuring the optical absorption in the UV–vis region or determining the positions of the band edges involved in electronic transitions by means of direct or inverse photoemission measurements. Sometimes the band gap can also be estimated from spectroscopic ellipsometry measurements or electron energy loss spectra.

On the computational side, there are two main problems related to the comparison of KS band gaps with experimental band gaps, namely (i) the neglect of excitonic effects and (ii) the approximations present in standard density functionals. The topic has been widely debated in various research articles,^{1–6} and it was recognized a long time ago that standard LDA or GGA functionals result in band gaps that are too small

as a result of the self-interaction problem.⁷ Meanwhile, a general consensus has been reached about the fact that hybrid functionals, in which a portion of exact exchange is added to the DFT exchange functionals, offer a better description of this important property.

The first reports showing the superior performances of hybrid functionals appeared in the literature 20 years ago and were based on the CRYSTAL code.^{8–10} This computer code was designed for the study of crystalline solids and is based on the use of localized basis functions.¹¹ This offers the advantage that the calculation of the exact exchange can be done at a very reasonable computational cost, at variance with plane-wave codes. However, it was only about 15 years ago that the superior performances of hybrid functionals in the description of insulators and semiconductors became generally accepted. An important step in this direction was the implementation of

Received: June 4, 2019

Published: October 15, 2019



ACS Publications

© 2019 American Chemical Society

6294

DOI: 10.1021/acs.jctc.9b00545

J. Chem. Theory Comput. 2019, 15, 6294–6312

hybrid functionals in popular plane-wave electronic structure codes such as VASP.¹² However, the cost of hybrid DFT calculations with plane-wave codes has partly limited, and still limits, the applicability of hybrid functionals to complex problems or large systems.

Hybrid functionals can be constructed by mixing a portion of the exact exchange energy E_x to GGA-type functionals (whose exchange and correlation contributions are denoted E_x^{GGA} and E_c^{GGA} , respectively); the general form of the exchange–correlation energy for one-parameter hybrid functionals is

$$E_{\text{xc}} = \alpha E_x + (1 - \alpha) E_x^{\text{GGA}} + E_c^{\text{GGA}} \quad (1)$$

Here the exact exchange energy is defined in analogy with Hartree–Fock theory, and the fraction of exact exchange, α , may vary from 0 to 1. Several hybrid functionals have been designed and tested; they usually differ in the choice of the GGA functional approximating the semilocal part and in the value of α .¹³ Historically, the first hybrid functional proposed is the popular B3LYP functional.¹⁴ B3LYP does not follow eq 1, being based on a three-parameter functional form fitted to reproduce a set of thermochemical data for molecules and incorporating 20% exact exchange ($\alpha = 0.20$). Later, the PBE0 functional was proposed,¹⁵ which builds on the original Becke's one-parameter hybrid, eq 1, using $\alpha = 0.25$. A formal justification for this α value was given on the basis of comparison with many-body perturbation theory.¹⁶ It should be noticed, however, that the validity of this argument is strictly limited to the reproduction of atomization energies of molecular data sets.

As we mentioned above, hybrid functionals proved to be quite efficient in reproducing the band gaps of insulators and semiconductors. Interestingly, they were also shown to better describe highly correlated rare-earth and transition metal oxides;^{17–20} in fact, these are Mott–Hubbard insulators, which are described to be metallic when semilocal functionals such as GGA are used, while introducing a portion of exact exchange in hybrids partially corrects the self-interaction error, yielding a qualitatively correct insulating ground state.

Hybrid functionals specifically tailored to solids have also been developed. In particular, range-separated (RS) hybrids were proposed and have since become increasingly popular in solid-state calculations.^{21,22} In RS hybrids, the Coulomb kernel in the exact exchange energy is separated into short- and long-range contributions, which are treated independently. In particular, two different exchange fractions, related to the short- and long-range parts of the energy, need to be introduced. A popular RS hybrid in which the long-range part of the Coulomb interaction is completely neglected (short-range hybrid) is the Heyd–Scuseria–Ernzerhof (HSE06) functional,²¹ for which the short-range exchange fraction α is set to 0.25.

A general assumption is that a fixed value of α (e.g., 0.20 for B3LYP, 0.25 for PBE0 and HSE06) does not ensure an equally accurate prediction of electronic properties of a very broad variety of materials. For instance, the band gaps of silicon and germanium are overestimated at the PBE0 level, but this overestimation is not systematic.³ An option to circumvent the problem is to consider the exact exchange fraction as a system-dependent term and not as a universal fixed amount. This leads to the so-called dielectric-dependent (DD) functionals.^{23–26} For DD hybrids, the exchange–correlation potential takes a

functional form similar to eq 1, but with an exchange fraction that is system-dependent and in particular is a function of the static dielectric constant of the material:

$$\alpha = \frac{1}{\epsilon_{\infty}} \quad (2)$$

In these methods, α depends on the approximations made in computing the dielectric constant ϵ_{∞} or on the accuracy of the experimental measurements if ϵ_{∞} is taken from experiment (in this case, the method has some empirical flavor due to the use of an external parameter). The other approach is to compute the dielectric constant taking an initial α value, from this generate a new dielectric-dependent α , then iterate the procedure until self-consistency is achieved and a theoretical value of ϵ_{∞} is obtained under a finite electric field using a coupled perturbed technique. In this latter case, the method can be considered as parameter-free, fully ab initio.

Recently, Chen et al.²⁷ presented a general scheme to determine case by case the exchange mixing parameter in the long-range region, as well as the range separation, on the basis of a calculation of the dielectric constant. This nonempirical dielectric-dependent scheme was then tested on 32 insulators and semiconductors, including 10 oxides.²⁸ However, a systematic study of a large set of oxides and hydroxides on an equal footing in which standard, dielectric-dependent, and range-separated dielectric-dependent functionals are compared is, to the best of our knowledge, still lacking.

In this work we attempt to fill the gap by computing the band gaps of two classes of materials: (i) a series of 24 bulk three-dimensional (3D) oxides ranging from small-gap (~2.4 eV) semiconductors to large-gap (~10.6 eV) insulators and (ii) a group of 24 bulk two-dimensional (2D) layered materials (with van der Waals gap, so-called quasi-2D materials) that includes oxides but also hydroxides, nitrides, sulfides, chlorides, oxyhalides, and tellurides. We then perform a statistical analysis of the first-principles-calculated results. We compare seven kinds of hybrid functionals, including three global hybrid functionals (PBE0, B3LYP, and DD-B3LYP) and four range-separated hybrid functionals (HSE06, SC-BLYP, DD-SC-BLYP, and DD-CAM-B3LYP), and we discuss their performances in reproducing both the band gap and the dielectric constant of these 3D and 2D materials. We will show that the use of DD functionals is beneficial only for the quasi-2D materials, while it does not provide a systematic improvement and computational advantage for the 3D bulk oxides.

The conclusions of the present research work are further corroborated by a principal component analysis (PCA)^{29,30} based on the structural parameters and computed results from the seven different kinds of hybrid functionals mentioned above to rationalize the main apparent and/or hidden correlations between the accuracy of the estimated band gaps and the properties of these materials.

2. COMPUTATIONAL DETAILS

All of the calculations reported in this work are based on hybrid functionals in which the fraction of exact Fock exchange was calculated within the coupled perturbed Hartree–Fock/Kohn–Sham (CPHF/KS)^{31–33} method as implemented in the CRYSTAL17 program.³⁴ The code makes use of a linear combination of atomic orbitals and Gaussian-type basis sets to construct the wave function of the system. An all-electron basis set was used for the O atom; all-electron or scalar relativistic

Table 1. Structures, Experimental Band Gaps (E_g), Methods of Measurement, and References for the Series of 24 3D Metal Oxides Considered in This Study^a

oxide (space group no.)	E_g (eV)	method	oxide (space group no.)	E_g (eV)	method
hexagonal BeO (186)	10.6 [D]	reflectance spectra, 77 K ⁴¹	cubic In ₂ O ₃ (206)	4.10 [D]	optical absorption edge, 300 K ⁶⁵
	~15.0 [OG]	optical absorption ⁴²		3.72 [D]	ARPES measurement, 300 K ⁶⁶
trigonal SiO ₂ (154)	9.10 [I]	UV exciton absorption edge ⁴³	tetragonal SnO ₂ (136)	3.75 [D], 2.62 [I]	optical absorption spectra ⁶⁷
	13.33 [D]	spectroscopic ellipsometry ⁴⁴		3.60 [D]	two-photon spectra/ absorption, 7 K ⁶⁸
trigonal Al ₂ O ₃ (167)	8.8 [D]	UV absorption ⁴⁵	3.75 [D]	absorption spectra, 77 K ⁶⁹	
	8.55 [D]	transmittance and reflectance, 300 K ⁴⁶		2.6 [I]	photoluminescence, 4.2 K ⁷⁰
trigonal B ₂ O ₃ (144)	12.4 [D]	spectroscopic ellipsometry ⁴⁷	hexagonal ZnO (186)	3.44 [D]	transmission spectra, 4.2 K ⁷¹
	7.2 [D]	transmittance spectra ⁴⁸		3.38 [D]	photoluminescence, 2 K ⁷²
	8.0 [I]	UV absorption ⁴⁹		3.3 [D]	UV-vis absorption, 300 K ⁷³
cubic Li ₂ O (225)	7.99 [D]	UV reflectance, 15 K ⁵⁰	monoclinic WO ₃ (14)	3.38 [D]	UV-inverse photoemission ⁷⁴
	6.6 [D]	optical absorption edge ⁵¹		3.52 [D], 2.62 [I]	photoelectrolysis spectra ⁷⁵
cubic MgO (225)	7.83 [D]	thermorelectance, 85 K ⁵²	cubic SrTiO ₃ (221)	3.25 [I], 3.75 [D]	VEELS, UV-absorption using ellipsometry ⁷⁶
	8.7 [D]	UV diffuse reflectance, 300 K ⁵³		3.20 [OG]	UV-vis reflectance, EELS (bulk) ⁷⁷
cubic CaO (225)	7.10 [D]	optical absorption spectra, 300 K ⁵⁴	cubic CeO ₂ (225)	3.3 [I], 3.6 [D]	spectroscopic ellipsometry, XPS (films) ⁷⁸
	7.5 [OG]	thermorelectance, 85 K ⁵²		3.20 [I]	X-ray photoemission ⁷⁹
cubic SrO (225)	5.90 [D]	optical absorption spectra, 20–300 K ⁵⁵	tetragonal a-TiO ₂ (141)	3.44 [I]	transmittance spectra/ absorption edge, 4.2 K ⁸⁰
	5.71 [D]	reflectance spectra, 55 K ⁵⁶		3.20 [D]	X-ray photoemission ⁷⁹
	5.77 [D]	emission/absorption spectra, 113 K ⁶⁴	tetragonal r-TiO ₂ (136)	3.03 [D]	transmittance spectra/ absorption edge, 1.6 K ⁸¹
monoclinic ZrO ₂ (14)	5.83 [D]	optical absorption edge, 300 K ⁶⁵		3.06 [D]	monoclinic BiVO ₄ (15)
	5.3 [D]	VUV spectroscopy and XPS ⁵⁷	cubic Cu ₂ O (224)	2.56 [I], 2.7 [D]	UV-vis spectra using VASE ⁸²
monoclinic HfO ₂ (14)	5.68 [D]	EELS ⁵⁸		2.4 [OG]	UV-vis DRS ⁸³
	5.77 [D]	UV-vis–NIR spectra (film) ⁵⁹		2.38 [D]	transmittance spectra ⁸⁴
tetragonal GeO ₂ (136)	5.35, 6.0 [D]	spectroscopic ellipsometry (film) ⁶⁰	2.17 [D]	2.17 [D]	optical absorption spectra, 5 K ⁸⁵
	4.4–5.8 [D]	optical absorption spectra ⁶¹		2.50 [D]	UV-vis–NIR absorption spectra, 300 K ⁸⁶
monoclinic Ga ₂ O ₃ (12)	4.85 [I], 4.9 [D]	ARPES measurement, 300 K ⁶⁶	2.17 [D]	2.17 [D]	
	4.43 [I], 4.48 [D]	transmittance and reflectance, 300 K ⁶³		2.17 [D]	
cubic BaO (225)	3.88 [D]	emission/absorption spectra, 113 K ⁶⁴			

^aStructures are ordered by decreasing band gap. Abbreviations: [D], direct band gap; [I], indirect band gap; IPES, inverse photoemission spectra; EELS, electron energy loss spectra; OG, optical band gap; VASE, variable-angle spectroscopic ellipsometry.

pseudopotentials and associated basis sets were adopted for the other atoms. The stability of the results with respect to the basis set was carefully checked in some cases, where the Pople triple- ζ basis set (commonly adopted for CRYSTAL calculations) was compared to Ahlrichs' TZVP basis set reoptimized for periodic calculations.³⁵ This ensured that the reported results are largely independent of the basis set chosen and that the conclusions can be generalized to other computational approaches based on plane-waves. A more thorough comparison of several effective core potentials and all-electron basis set in calculating the electronic structures of several oxides was previously reported and showed the robustness of the results with respect to the choice of the basis set.⁴ The complete list of basis sets adopted for each metal cation is reported in Table S1 in the Supporting Information.

The cutoff values for Coulomb and exchange integrals in self-consistent field calculations were 10^{-8} for the Coulomb overlap tolerance, Coulomb penetration tolerance, exchange overlap tolerance, and exchange pseudo-overlap in direct space and 10^{-18} for the exchange pseudo overlap in reciprocal space. However, in some specific cases, limiting their choice of the particular basis set for hybrid-type calculations, these convergence criteria were set to 10^{-10} and 10^{-30} , respectively. The SCF calculations were considered converged when the difference in energy between two subsequent cycles was less than 10^{-8} au. The k-point mesh was set with a shrinking factor of 8 for Pack-Monkhorst methods.

For all of the calculations, the experimental lattice constants and ionic positions were adopted for each oxide (see Table S2 for details). This can introduce some minor fluctuations in the values of the band gaps with respect to calculations where the

Table 2. Band Gaps Computed with Different Functionals for a Series of 24 Bulk 3D Metal Oxides (For Experimental Data, Also See Table 1) from Hybrid Density Functional Approaches (DD = Dielectric-Dependent); The Optimized Fock Exchange (α_{opt}) for DD Functionals Is Also Given

oxide (space group no.)	global hybrid				range-separated hybrid						expt
	PBE0 ($\alpha = 25\%$)	B3LYP ($\alpha = 20\%$)	DD-B3LYP	$\alpha_{\text{opt}}\ (%)$	HSE06 ($\alpha = 25\%$)	SC-BLYP ($\alpha = 20\%$)	DD-SC-BLYP	$\alpha_{\text{opt}}\ (%)$	DD-CAM-B3LYP	$\alpha_{\text{opt}}\ (%)$	
BeO (186)	10.45	10.23	13.64	48.8	9.73	9.71	12.12	48.9	9.86	44.5	10.6 [D]
SiO ₂ (154)	9.21	8.68	12.09	50.7	8.46	8.13	10.74	50.1	8.34	45.6	9.1 [I]
Al ₂ O ₃ (167)	8.83	8.55	10.49	38.3	8.15	8.05	9.54	38.4	7.73	34.0	8.8 [D]
B ₂ O ₃ (144)	9.36	8.86	11.41	42.3	8.59	8.28	10.18	42.5	8.09	36.5	8.0 [I]
Li ₂ O (225)	8.02	7.78	10.07	43.9	7.30	7.29	8.99	44.3	6.79	37.8	7.99 [D]
MgO (225)	7.39	7.12	9.63	44.6	6.74	6.65	8.57	44.8	6.50	39.0	7.83 [D]
CaO (225)	7.05	6.73	9.44	47.9	6.38	6.26	8.30	48.0	6.18	42.1	7.1 [D]
SrO (225)	5.47	5.17	6.31	32.7	4.76	4.65	5.46	32.8	3.97	26.7	5.90 [D]
ZrO ₂ (14)	6.37	5.92	6.26	23.6	5.67	5.38	5.61	23.4	4.79	20.4	5.83 [D]
HfO ₂ (14)	7.07	6.61	7.24	26.4	5.85	5.60	6.03	26.3	5.43	22.7	5.68 [D]
GeO ₂ (136)	4.80	4.28	5.57	31.4	4.10	3.75	4.71	31.4	3.35	27.3	5.35 [D]
Na ₂ O (225)	4.37	4.01	6.03	42.6	3.67	3.51	4.97	43.2	3.10	32.8	4.4–5.8 [D]
Ga ₂ O ₃ (12)	5.23	4.80	6.35	34.5	4.55	4.30	5.46	34.6	3.74	28.7	4.85 [I]
BaO (225)	4.00	3.74	4.59	30.6	3.28	3.23	3.80	30.6	2.46	24.6	3.88 [D]
In ₂ O ₃ (206)	4.07	3.70	4.89	32.8	3.39	3.22	4.08	32.8	2.46	26.0	3.72 [D]
SnO ₂ (136)	3.51	3.05	4.24	31.5	2.91	2.61	3.49	31.4	2.05	26.1	3.60 [D]
ZnO (186)	3.70	3.31	4.71	33.7	3.06	2.84	3.87	33.6	1.40	22.3	3.44 [D]
WO ₃ (14)	3.69	3.34	3.45	21.4	3.00	2.81	2.87	21.2	2.48	18.9	3.38 [D]
SrTiO ₃ (221)	4.01	3.60	3.67	20.8	3.33	3.08	3.12	20.6	2.56	17.8	3.25 [I]
CeO ₂ (225)	4.33	3.80	3.76	19.6	3.65	3.27	3.22	19.2	3.36	18.7	3.20 [I]
a-TiO ₂ (141)	4.22	3.77	3.72	19.4	3.58	3.29	3.24	19.2	2.77	17.6	3.20 [I]
r-TiO ₂ (136)	4.02	3.56	3.26	16.6	3.34	3.05	2.82	16.3	2.50	14.5	3.03 [D]
BiVO ₄ (15)	3.82	3.50	3.38	18.4	3.17	3.00	2.91	18.0	2.65	15.8	2.56 [I]
Cu ₂ O (224)	2.59	2.26	3.52	34.2	2.03	1.84	2.69	32.9	1.20	19.1	2.38 [D]
MAE (eV) ^a	0.53	0.46	1.25	—	0.59	0.66	0.58	—	1.03	—	0
MAPE (%) ^a	13.1	10.1	22.6	—	12.0	13.0	9.7	—	22.4	—	0
SD (eV) ^a	0.64	0.61	0.95	—	0.62	0.58	0.72	—	0.68	—	0
linear fit slope	0.911	0.922	1.317	—	0.899	0.915	1.213	—	0.997	—	1
linear fit intercept	0.799	0.358	-0.439	—	0.162	-0.131	-0.758	—	-0.982	—	0

^aAbbreviations: MAE, mean absolute error; MAPE, mean absolute percentage error; SD, standard deviation.

geometry (both atomic coordinates and lattice parameters) is fully optimized. However, this is not expected to affect the general conclusions about the performance of the various functionals considered, as the geometry optimization does not result in major changes in the computed band gaps. This aspect was checked in selected cases, as reported in Table S3.

The calculations were performed using the PBE0, B3LYP, HSE06, and SC-BLYP standard hybrid functionals, as mentioned above. It should be noticed that SC-BLYP displays a short-range separation formalism analogous to that of HSE06. These two functionals differ only in the exchange–correlation part (PBE plus 25% exact Fock exchange for HSE06; BLYP plus 20% Fock exchange for SC-BLYP). Short-range hybrids have the additional advantage of having a lower cost for solids because of the faster decay of the exchange interaction. This is true also for plane-wave codes, for which a calculation with a short-range hybrid requires fewer k-points than a long- or full-range hybrid.

For the dielectric-dependent functionals, we decided to use the B3LYP formulation and to determine self-consistently the portion of exact exchange, α . For the range-separated DD hybrid functionals, since the functional's derivatives (which are necessary to calculate the dielectric tensor as in the CPKS approach) are not yet implemented in the CRYSTAL17 code

for HSE06, we used the DD-SC-BLYP and DD-CAM-B3LYP functionals. This latter Coulomb attenuating method (CAM)-type functional combines the LYP exchange–correlation functional, including 20% Fock exchange as in B3LYP, with the long-range correction presented by Tawada et al.³⁶ The CAM-B3LYP functional in standard form comprises 0.19 exact exchange plus 0.81 Becke 1988 (B88) exchange interaction at short range and 0.65 exact exchange plus 0.35 B88 at long range. The intermediate region is smoothly described through the standard error function with a screening parameter of 0.33. The method was introduced to improve the description of the exchange–correlation functional tail compared with standard DFT or HF with long-range-corrected (LC) functionals.³⁷ The method is extremely successful on the basis of the molecular atomization energy of the G2 data set.³⁸

3. RESULTS AND DISCUSSION

3.1. 3D Metal Oxides. Since our analysis is based on a direct comparison of the KS DFT band gaps with experimentally measured values, it is important to discuss briefly the nature of computed and experimental band gaps. Most experimental band gaps are obtained from optical measurements, and because of excitonic effects, optical band gaps are generally smaller than electronic band gaps. In

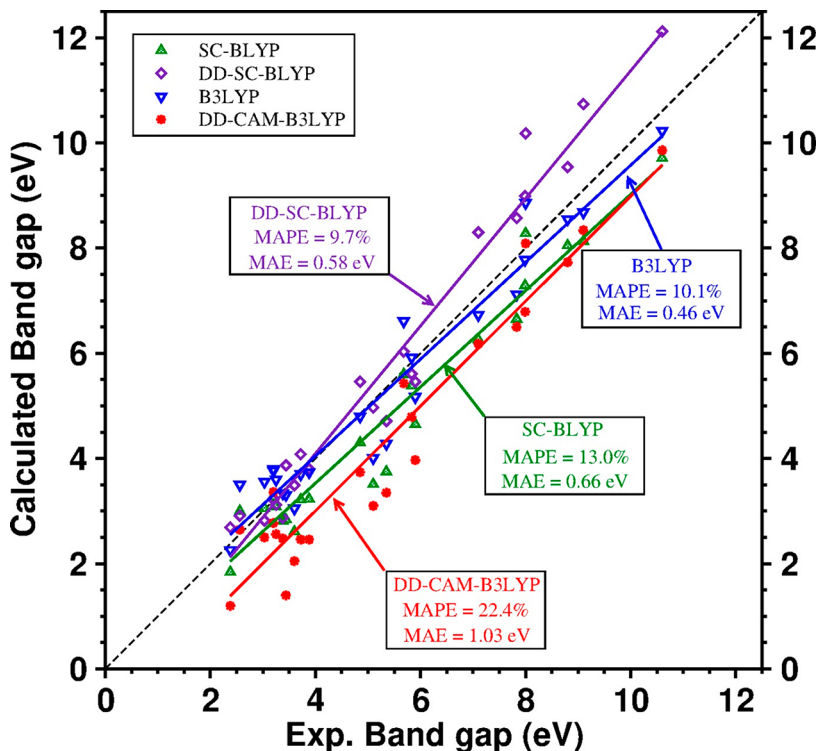


Figure 1. Correlations between computed and measured band gaps for a series of 24 3D metal oxides from various hybrid functionals (see Table 2).

transition metal oxides, the exciton binding energy can vary from a few millielectronvolts to several tenths of an electronvolt.^{39,40} In this respect, comparing KS band gaps with optical band gaps is a rather crude approximation, and one should not necessarily expect a one-to-one correspondence between the two values. In other cases, experimental band gaps are derived from photoemission experiments, where electrons are removed from or added to the system, resulting in large relaxation energies. Finally, the nature of the band gap can be direct or indirect, and this also affects the comparison in some cases. For this reason, in the analysis of the computed KS band gaps and comparison with experimental values, we specify which method has been used to measure the band gap, and its nature, when available (see Table 1). A one-to-one comparison is proposed here between the available type of band gap (either direct or indirect) and the corresponding calculated direct or indirect value. When more than one experimental value exists, for the comparison with the theoretical data and the calculation of the errors we rely on the most recent measurements on crystalline materials.

3.1.1. Standard Hybrids: PBE0, B3LYP, HSE06, and SC-BLYP. We start by analyzing some standard hybrid functionals with fixed amounts of exact exchange (25% in PBE0 and HSE06 and 20% in B3LYP and SC-BLYP; see Table 2). Two of these functionals, PBE0 and B3LYP, are global hybrid functionals, while the other two, HSE06 and SC-BLYP, are short-range-separated hybrid functionals, as discussed earlier.

In general, PBE0 performs well for the bulk 3D oxides, with errors smaller than 1 eV for most compounds. PBE0 generally overestimates the band gap, with the exceptions of SnO₂ (3.51 vs 3.6 eV), MgO (7.39 vs 7.83 eV), SrO (5.47 vs 5.90 eV), Na₂O (4.37 vs 4.4–5.8 eV), and GeO₂ (4.80 vs 5.35 eV). However, PBE0 gives excellent results for systems with very large gaps, i.e., BeO (10.45 vs 10.6 eV), SiO₂ (9.21 vs 9.1 eV),

and Al₂O₃ (8.83 vs 8.8 eV), consistent with previous reports.² The mean absolute error (MAE) for PBE0 is 0.53 eV, while the mean absolute percentage error (MAPE) is 13.1%. The standard deviation (SD) is 0.64 eV.

Not surprisingly, B3LYP gives oxide band gaps that are a bit smaller than the PBE0 values because of the lower amount of exact exchange in the functional. In particular, for a large number of materials the computed band gaps are very close to the experimental ones. For example, Al₂O₃, B₂O₃, Li₂O, CaO, ZrO₂, HfO₂, GeO₂, Ga₂O₃, BaO, In₂O₃, ZnO, WO₃, SrTiO₃, and Cu₂O are materials whose band gaps are well-reproduced by this functional. A critical case is seen for BiVO₄, where the band gap is overestimated by 1 eV, consistent with the previous theoretical results.⁸⁷ A remarkable overestimate (~0.5 eV) is reported also for rutile and anatase TiO₂ and CeO₂. The MAE for B3LYP, 0.46 eV, is a bit smaller than that for PBE0; also, the MAPE, 10.1%, is slightly better (see Table 2).

HSE06 in general gives good values for materials with band gaps up to 3–4 eV, while a general underestimate is reported for large-gap insulators such as BeO (9.73 eV HSE06, 10.6 eV expt), SiO₂ (8.46 eV HSE06, 9.1 eV expt), Al₂O₃ (8.15 eV HSE06, 8.8 eV), Li₂O (7.30 eV HSE06, 7.99 eV expt), MgO (6.74 eV HSE06, 7.83 eV expt), SrO (4.76 eV HSE06, 5.90 eV expt), GeO₂ (4.10 eV HSE06, 5.35 eV expt), Na₂O (3.67 eV HSE06, 4.4–5.8 eV expt), and Cu₂O (2.03 eV HSE06, 2.38 eV expt). On the other side, HSE06 gives a better estimate of the B₂O₃ band gap (8.59 eV vs 8.0 eV expt) compared with PBE0. Even though the situation improves for BiVO₄ compared with PBE0 or B3LYP, HSE06 is still off here (3.17 eV HSE06, 2.56 eV expt). Overall, the MAE, 0.59 eV, is similar to those of PBE0 and B3LYP, as is the MAPE, 12.0%.

The SC-BLYP band gaps are, not surprisingly, similar to the HSE06 ones but a bit smaller because of the smaller α value. Overall, the MAE, 0.66 eV, is the largest considered so far, and

Table 3. Dielectric Constants Computed with Different Functionals for the Series of 24 3D Metal Oxides (For Experimental Data, Also See Table 4)

oxide (space group no.)	global hybrid			range-separated hybrid			expt
	PBE0 ($\alpha = 25\%$)	B3LYP ($\alpha = 20\%$)	DD-B3LYP	SC-BLYP ($\alpha = 20\%$)	DD-SC-BLYP	DD-CAM-B3LYP	
BeO (186)	2.17	2.15	2.05	2.15	2.04	2.25	2.95
SiO ₂ (154)	2.08	2.08	1.97	2.08	1.96	2.2	2.3
Al ₂ O ₃ (167)	2.75	2.72	2.61	2.72	2.60	2.94	3.4
B ₂ O ₃ (144)	2.49	2.50	2.36	2.50	2.35	2.73	2.19
Li ₂ O (225)	2.44	2.41	2.28	2.40	2.26	2.64	2.68
MgO (225)	2.40	2.38	2.24	2.38	2.23	2.56	2.95
CaO (225)	2.23	2.23	2.09	2.22	2.08	2.38	3.27
SrO (225)	3.23	3.22	3.05	3.22	3.05	3.75	3.47
ZrO ₂ (14)	4.26	4.32	4.23	4.35	4.27	4.90	4.80
HfO ₂ (14)	3.87	3.90	3.78	3.92	3.79	4.41	4.41
GeO ₂ (136)	3.29	3.33	3.18	3.34	3.19	3.66	4.43
Na ₂ O (225)	2.58	2.58	2.34	2.57	2.32	3.05	NA
Ga ₂ O ₃ (12)	3.05	3.07	2.89	3.08	2.89	3.49	3.5
BaO (225)	3.45	3.43	3.27	3.43	3.27	4.08	3.68
In ₂ O ₃ (206)	3.22	3.25	3.05	3.26	3.05	3.86	4.00
SnO ₂ (136)	3.30	3.37	3.17	3.38	3.18	3.83	4.06
ZnO (186)	3.18	3.22	2.96	3.24	2.97	4.48	3.73
WO ₃ (14)	4.61	4.70	4.66	4.76	4.72	5.31	4.81
SrTiO ₃ (221)	4.71	4.83	4.80	4.88	4.86	5.62	6.1
CeO ₂ (225)	4.82	5.07	5.10	5.17	5.23	5.35	5.52
a-TiO ₂ (141)	4.92	5.12	5.15	5.19	5.23	5.83	5.62
r-TiO ₂ (136)	5.57	5.83	6.04	5.92	6.15	6.89	7.37
BiVO ₄ (15)	5.30	5.38	5.44	5.48	5.55	6.32	9.6
Cu ₂ O (224)	3.30	3.44	2.93	3.52	3.03	5.25	6.46
MAE	0.92	0.87	0.97	0.84	0.94	0.56	0
MAPE (%)	19.4	18.5	21.1	18.0	20.7	12.6	0

the MAPE is 13%. Thus, the performances of the four functionals can be considered quite similar. This is also shown by the similar slopes of the linear fits of the interpolating curves, which are all close to 0.9 (Table 2 and Figure 1). On the contrary, the intercepts are quite different, with the range-separated functionals giving intercepts close to zero (0.16 HSE06, -0.13 SC-BLYP), followed by B3LYP (0.36) and PBE0 (0.80) (Table 2). Plots of the band gaps calculated with all of the functionals for bulk 3D metal oxides are given in Figure S1.

Having considered the results for hybrid functionals with a fixed portion of exact exchange, we move now to the band gaps for the same set of bulk 3D metal oxides computed with various DD hybrid functionals, where a certain portion of exact exchange at either short or long range is determined self-consistently for every material (material-dependent).

3.1.2. Dielectric-Dependent Hybrids: DD-B3LYP, DD-SC-BLYP, and DD-CAM-B3LYP. In this section, we consider three functionals where α is determined self-consistently from the inverse of the high-frequency dielectric constant. One of these functionals, DD-B3LYP, is a global hybrid, while the other two, DD-SC-BLYP and DD-CAM-B3LYP are short- and long-range-separated hybrid functionals, respectively. Because of technical limitations in the CRYSTAL code, it was not possible to calculate the high-frequency dielectric constant with the HSE06 functional. However, this does not diminish the general validity of our data set given the substantial similarity between HSE06 and SC-BLYP (vide supra). In the DD approach, the static dielectric constant of the material was calculated self-consistently (see section 2) and used to determine the α parameter. We also compare the computed ϵ_{∞} values with the

measured static dielectric constants (see Table 3). Since several methods can be used to measure the dielectric constant, in Table 4 we report the detailed information about the experimental methods adopted and the corresponding references whenever available (for some oxides this quantity does not seem to be available).

In DD-B3LYP, α varies from a maximum of 0.507 in SiO₂ to a minimum of 0.166 in r-TiO₂ (Table 2). The results of the band gap calculations at the DD-B3LYP level (Table 2), can be considered somewhat disappointing. While for some compounds there is an improvement, such as for SrO (5.90 eV expt, 5.17 eV B3LYP, 6.31 eV DD-B3LYP), no substantial or systematic improvement is found, and in some cases there is a clear deterioration of the results. For instance, for ZnO (experimental band gap of 3.4 eV), B3LYP gives a reasonable estimate of 3.31 eV while DD-B3LYP predicts a gap of 4.71 eV, which is off by 1.3 eV! Another example is that of In₂O₃, where B3LYP perfectly matches the experimental band gap of 3.7 eV while the DD variant predicts a gap of 4.89 eV. Even worse is the case of BeO, where the self-consistent $\alpha = 0.488$ leads to a very large gap of 13.64 eV, which is overestimated by 3 eV with respect to the experiment value (Table 2). Thus, the tendency of DD-B3LYP to overestimate the band gap is more pronounced for large-gap insulators. The general deterioration of the results going from the “empirical” B3LYP functional to DD-B3LYP is clearly shown by the MAE of 1.25 eV (Table 2), which is 2.7 times larger than that of B3LYP. Also the slope of the linear fit, 1.32, is worse (Table 2). Therefore, it is not at all clear that a DD functional leads to a general improvement in the band gaps of 3D metal oxides compared with a standard B3LYP calculation.

Table 4. Experimental Static Dielectric Constants, ϵ_{∞} , for the Series of 24 3D Metal Oxides Considered in This Work (NA = Not Available)

oxide (space group no.)	ϵ_{∞}	method
hexagonal BeO (186)	2.95	$\epsilon_{\infty} = n^2$ relation ⁸⁸
trigonal SiO ₂ (154)	2.3	spectroscopic ellipsometry ^{89,90}
trigonal Al ₂ O ₃ (167)	3.4	not mentioned ^{91,92}
trigonal B ₂ O ₃ (144)	2.19	^a phonon frequency, $\epsilon_{\infty} = n^2$ relation ⁹³
cubic Li ₂ O (225)	2.68	not mentioned ⁹⁴
cubic MgO (225)	2.95	^b infrared absorption, estimated using ϵ_0 ⁹⁵
cubic CaO (225)	3.27	capacitance measurement estimated using ϵ_0 ⁹⁶
cubic SrO (225)	3.47	^c $\epsilon_{\infty} = n^2$ relation ⁹⁷
monoclinic ZrO ₂ (14)	4.80	^d $\epsilon_{\infty} = n^2$ relation ⁹⁸
monoclinic HfO ₂ (14)	4.41	$\epsilon_{\infty} = n^2$ relation ⁵⁹
tetragonal GeO ₂ (136)	4.43	ellipsometry measurement ⁹⁹
monoclinic Ga ₂ O ₃ (12)	3.57	fit of the Cauchy dispersion model to the $\epsilon_{\infty} = n^2$ relation ^{100,101}
	3.46	^e $\epsilon_{\infty} = n^2$ relation ¹⁰²
cubic BaO (225)	3.68	Sellmeier dispersion energy, phonon frequencies ^{103,104}
cubic In ₂ O ₃ (206)	4.00	spectroscopic transmittance and reflectance ¹⁰⁵
tetragonal SnO ₂ (136)	4.06	not mentioned ²
hexagonal ZnO (186)	3.73	^f SE and Raman scattering ¹⁰⁶
monoclinic WO ₃ (14)	4.81	$\epsilon_{\infty} = n^2$ relation ¹⁰⁷
cubic SrTiO ₃ (221)	6.1	not mentioned ^{91,92}
cubic CeO ₂ (225)	5.52	^g EELS, $\epsilon_{\infty} = n^2$ relation ⁷⁷
	6.10	^h VASE, $\epsilon_{\infty} = n^2$ relation ⁷⁸
tetragonal a-TiO ₂ (141)	5.62	infrared reflectivity and phonon modes ^{108,109}
tetragonal r-TiO ₂ (136)	7.37	$\epsilon_{\infty} = n^2$ relation ¹¹⁰
monoclinic BiVO ₄ (15)	3.6–4.1	infrared reflectivity spectroscopy UV-vis spectroscopy ¹¹¹
	9.6	^h VASE ⁸²
cubic Cu ₂ O (224)	6.46	reflectivity and dispersion, $\epsilon_{\infty} = n^2$ relation ^{112,113}
cubic Na ₂ O (225)	NA	

^aEstimated at using the relation $\epsilon_{\infty} = n^2$, where n is the refractive index. ^bThe low-frequency dielectric constant, ϵ_0 , is 9.42, which gives $\epsilon_{\infty} = 2.95$. ^cFrom capacitance measurement at low frequency (1–10 kHz) giving $\epsilon_0 = 14.5$, then refractive index measurement at 656.3 to 404.7 nm. ^dFrom Raman scattering and measurement of the refractive index, n . ^eFrom measurement of the refractive index, n , for films at wavelength $\lambda = 980$ nm and direct band gap of 4.4 eV. ^fSpectroscopic ellipsometry (SE). ^gSpectroscopic measurement from electron energy loss spectra (EELS) on a single crystal. ^hEstimation of ϵ_{∞} from variable-angle spectroscopic ellipsometry (VASE) measurement of the refractive index of the film ($\lambda = 200$ nm).

One can expect that this is reflected in corresponding variations of the static dielectric constants. The results for the dielectric constants (Table 3) show a considerable scatter of values, with some deviations from experiment. The PBE0 and B3LYP results are usually quite close to each other, as shown by the similar MAE values (0.92 eV and 0.87 eV; Table 3). The scatter is not better for DD-B3LYP, with a MAE of 0.97 eV (Table 3). The MAPE is around 20% for all three functionals. A typical case is represented by CaO. Here the experimental value of ϵ_{∞} is 3.27, to be compared with the computed values 2.23 (B3LYP) and 2.09 (DD-B3LYP). The error is about 50% for the standard functional and is even larger for the DD functional. This error is reflected in a large

fraction of exact exchange (48%) and an overestimate of the band gap (9.44 eV vs 7.1 eV expt) (Table 2).

We consider now the band gaps computed with the two DD range-separated functionals, DD-SC-BLYP and DD-CAM-B3LYP (Table 2). First of all, we noticed that the self-consistently determined amount of Fock exchange is quite similar for the range-separated DD-SC-BLYP and global DD-B3LYP functionals. DD-SC-BLYP performs very well for all of the 3D oxides with band gaps smaller than 5–6 eV. Here the errors are relatively small, and there are no odd cases. For large-gap insulators there is a tendency to overestimate the band gaps, with errors that can be up to 1.5–1.6 eV in absolute value (BeO and SiO₂). In general, however, the functional performs quite well, giving a MAE of 0.58 eV and a MAPE of 9.7%. The slope of the linear fit is 1.21, and the intercept is −0.76. Also, the SD (0.72 eV) is reasonably small for DD-SC-BLYP (though a bit larger than for SC-BLYP, 0.58 eV). If we compare these data with those obtained using the standard B3LYP and HSE06 functionals (Table 2), we see no real improvement in using a DD functional: the MAE is similar or larger and the MAPE is slightly better, but the linear fit is definitely worse. In short, there is no systematic improvement in using the DD-SC-BLYP functional. If we look at the computed dielectric constants, DD-SC-BLYP provides a MAE of 0.94, which is similar to that of the other functionals (Table 3). Actually, both the MAE and MAPE of DD-SC-BLYP are worse than the corresponding values for the SC-BLYP method, in which the contribution of exact exchange is fixed. In this respect, it is not surprising that the band gaps are also reproduced with similar errors.

Finally, we consider DD-CAM-B3LYP. This functional provides the best correspondence with the measured dielectric constants (MAE = 0.56; Table 3), despite some odd cases. The largest deviation is found for BiVO₄, where the computed ϵ_{∞} is 6.32 versus experimental estimates that go from 3.6–4.1 to 9.6 (Table 4), showing that there is some uncertainty in the experimental evaluation of the dielectric constant of this material. Considering the smaller MAE for the dielectric constants, one should expect an improvement in the description of the band gaps using the DD-CAM-B3LYP functional. However, the results do not show such a trend (see Table 2). The first observation is that α varies from a minimum of 0.145 for rutile TiO₂ to a maximum of 0.456 for SiO₂, with a similar range as for the DD-B3LYP functional. However, for many systems the optimal α remains close to 0.20, i.e., close to the B3LYP value (Table 2). Large values of α are found for the large-gap insulators, from B₂O₃ to CaO (Table 2). Indeed, the band gap of B₂O₃ is properly reproduced (8.09 eV DD-CAM-B3LYP, 8.0 eV expt). DD-CAM-B3LYP yields optimized values of α that are substantially smaller than those with DD-B3LYP or DD-SC-BLYP, leading to smaller band gaps as well. This mitigates the overestimation reported for large-gap insulators in the case of DD-B3LYP and DD-SC-BLYP.

However, besides these positive cases, a number of severe failures appear for smaller-band-gap systems: ZnO is predicted by DD-CAM-B3LYP to have a gap of 1.40 eV, which is 2 eV below the experimental value (3.44 eV); SnO₂ is predicted to have a gap of 2.05 eV, versus 3.60 eV experimentally; and in particular, Cu₂O has a computed gap of 1.20 eV, against an experimental value of 2.38 eV. For SrTiO₃ and WO₃, an underestimation of 1 eV is also noted. Overall, the few cases where there is an improvement are not sufficient to compensate for the several cases where there is a deterioration

Table 5. Structures, Experimental Band Gaps (E_g), Methods of Measurement, and References for the Series of 24 Quasi-2D Materials Considered in This Study^a

layered material (space group no.)	E_g (eV)	method
hexagonal 2H-BN (194)	5.96 [I]	photoemission and absorption spectra ¹¹⁷
trigonal CdCl ₂ (166)	5.8 [D]	EELS on films ^{118,119}
trigonal Mg(OH) ₂ (164)	5.7 [D], 7.0 [D]	UV-vis absorption spectra using a nanodisk sample, phototransmittance in films ^{120,121}
	3.5 [D]	UV-vis absorption using a nanostructured sample ¹²²
trigonal Ca(OH) ₂ (164)	4.5 [D]	not mentioned ¹²³
orthorhombic 1-TiO ₂ (63)	4.25 [D]	UV-vis-NIR absorption spectra ¹²⁴
trigonal CdI ₂ (164)	3.2–3.25 [I] 3.0 [I], 3.6 [D]	optical absorption and normal-incidence reflectivity ¹²⁵ optical absorption on films ¹²⁶
	3.8 [D]	EELS on films ¹¹⁸
tetragonal BiOCl (129)	3.18 [I] 3.20 [I]	UV-vis DRS ¹²⁷ UV-vis DRS ¹²⁸
	3.30 [I]	UV-vis absorption spectra, VB emission ¹²⁹
hexagonal 2H-GaS (194)	2.86 [I], 2.92 [D]	PA and MA spectra ¹⁵¹
	3.05 [D]	optical absorption and electroabsorption ¹³⁰
orthorhombic V ₂ O ₅ (59)	2.30 [I] 2.8 [D]	transmittance spectra/absorption edge ¹³¹ emission spectra (UPS, IPES) ¹³²
trigonal 1T-SnS ₂ (164)	2.1 [I], 2.3 [D] 2.07 [I], 2.88 [D]	optical absorption/transmittance spectra ¹³³ optical absorption, single crystal, 300 K ¹³⁴
	2.25 [I]	transmittance and reflectance, thin-film ¹³⁵
	2.28 [I], 2.38 [D]	optical absorption spectra and IPES on a single crystal ¹³⁶
orthorhombic MoO ₃ (62)	2.20 [I] 2.8 [D] 3.27 [D]	UV-vis absorption spectra ¹³⁷ photocurrent, <i>I</i> – <i>V</i> curve ¹³⁸ X-ray photoemission ¹³⁹
tetragonal BiOI (129)	2.76 [I], 3.16 [D] 1.85 [I] 1.80 [I]	optical absorption/transmittance spectra ¹³³ UV-vis DRS ¹⁴⁰ UV-vis absorption spectra, VB emission ¹²⁹
trigonal 1T-ZrS ₂ (164)	1.6 [I], 1.4 [I] 2.27 [D1], 1.78 [I1]	reflectivity spectra at 77 K ^{141,159} Raman spectra, resonance Raman spectra ¹⁴²
trigonal 1T-HfS ₂ (164)	2.85 [I], 3.6 [D] 1.96 [I] 2.6 [D], 2.13 [I] 1.96 [I] 1.39 [I], 2.09 [D]	ARPES and IPES ¹⁴³ optical absorption and normal-incidence reflectivity ¹²⁵ resonance Raman spectrum ¹⁴² transmission spectra ¹⁴⁴ PA and MA spectra ¹⁵¹
triclinic 3R-ReS ₂ (2)	1.32 [OG] 1.33–1.4 [I] 1.37 [I], 1.55 [D]	optical spectra (no further information) ¹⁴⁵ optical absorption spectra of a single crystal ¹⁴⁶
hexagonal 2H-WS ₂ (194)	1.35 [I], 1.3 [I]	^a PA and MA spectra ¹⁵¹
tetragonal SnO (129)	1.30 [I], 2.7 [D]	photocurrent spectra, optical UV-vis absorption ^{147,150}
hexagonal 2H-MoS ₂ (194)	1.29 [I] 1.23 [I]	optical absorption and reflectance spectra ¹⁴⁸ ARPES at 300 K on a single crystal ¹⁴⁹
hexagonal 2H-WSe ₂ (194)	1.37 [I], 1.87 [D] 1.20 [I], 1.25 [I]	photocurrent spectra ¹⁵⁰ PA and MA spectra ¹⁵¹
hexagonal 2H-MoSe ₂ (194)	1.1 [I] 1.25 [I], 1.56 [D]	photocurrent spectra, SE on films ^{150,152} ARPES at 300 K single crystal ¹⁴⁹
trigonal 1T-HfSe ₂ (164)	1.1 [I] 1.13 [I] 1.21 [I], 1.49 [D]	PA and MA spectra ¹⁵¹ optical absorption ^{153,154}
trigonal 1T-SnSe ₂ (164)	0.97 [I], 1.62 [D] 0.98 [I], 1.63 [D]	optical absorption and normal-incidence reflectivity ¹²⁵ PA and MA spectra ¹⁵¹
hexagonal 2H-MoTe ₂ (194)	1.2 [D] 1.0 [I] 0.89 [I], 1.06 [D]	optical absorption, single crystal, 300 K ¹³⁴ reflectivity spectra, single crystal, 300 K ¹⁵⁵
trigonal 1T-TiS ₂ (164)	0.3 [I], 0.3 [I] SM	DRS on a thin film ¹⁵⁶ ARPES at 300 K single crystal ¹⁴⁹ PA and MA spectra ¹⁵¹ ARPES; reflectivity spectra at 77 K ^{157–160} X-ray emission spectra ¹⁶¹

^aStructures are ordered by decreasing band gap. Abbreviations: PA, photoacoustic; MA, modulated reflectance; [I], indirect band gap; [D], direct band gap; ARPES, angle-resolved photoemission spectroscopy; EELS, electron energy loss spectroscopy; DRS, diffuse reflectance spectra; IPES, inverse photoemission spectroscopy; SM, semimetal; SE, spectroscopic ellipsometry; VB, valence band.

Table 6. Band Gaps Computed with Different Functionals for a Series of 24 Quasi-2D Materials (For Experimental Data, Also See **Table 5**) from Hybrid Density Functional Approaches (DD = Dielectric-Dependent); The Optimized Fock Exchange (α_{opt}) for DD Functionals Is Also Given

layered material (space group no.)	global hybrid				range-separated hybrid						expt
	PBE0 ($\alpha = 25\%$)	B3LYP ($\alpha = 20\%$)	DD-B3LYP	$\alpha_{\text{opt}}\%)$	HSE06 ($\alpha = 25\%$)	SC-BLYP ($\alpha = 20\%$)	DD-SC-BLYP	$\alpha_{\text{opt}}\%)$	DD-CAM-B3LYP	$\alpha_{\text{opt}}\%)$	
2H-BN (194)	6.58	6.18	6.96	29.0	5.85	5.64	6.16	28.9	5.05	24.8	5.96 [I]
1T-CdCl ₂ (166)	5.95	5.44	7.60	45.0	5.26	4.95	6.46	45.1	4.94	38.2	5.8 [D]
1T-Mg(OH) ₂ (164)	6.83	6.40	9.52	49.3	6.12	5.91	8.30	49.6	5.77	42.5	5.7 [D]
1T-Ca(OH) ₂ (164)	6.87	6.38	9.96	54.4	6.15	5.89	8.61	54.8	5.97	47.4	4.5 [D]
l-TiO ₂ (63)	5.34	4.85	5.75	29.2	4.69	4.36	4.98	28.9	4.23	25.9	4.25 [D]
1T-CdI ₂ (164)	4.94	4.53	5.60	35.6	4.32	4.07	4.76	35.4	4.00	30.8	3.6 [D]
tet-BiOCl (129)	4.28	4.12	4.27	22.2	3.62	3.62	3.70	22.0	3.03	18.8	3.18 [I]
2H-GaS (194)	3.83	3.39	3.65	23.8	3.21	2.96	3.11	23.6	2.53	20.8	3.05 [D]
α -V ₂ O ₅ (59)	3.76	3.31	3.57	23.0	3.12	2.81	2.96	22.5	2.48	20.5	2.3 [I]
1T-SnS ₂ (164)	2.71	2.35	2.00	14.5	2.06	1.87	1.64	14.1	1.22	11.8	2.28 [I]
α -MoO ₃ (62)	4.10	3.71	4.05	24.4	3.45	3.23	3.43	23.9	3.03	21.5	2.2 [I]
tet-BiOI (129)	2.63	2.43	2.27	16.9	2.03	1.96	1.87	16.6	1.58	14.6	1.80 [I]
1T-ZrS ₂ (164)	2.42	2.16	1.76	13.4	1.78	1.67	1.43	12.9	1.13	10.8	1.4 [I]
1T-HfS ₂ (164)	2.64	2.38	2.09	15.1	1.99	1.90	1.71	14.8	1.30	12.2	1.39 [I]
3R-ReS ₂ (2)	2.16	1.83	1.17	7.6	1.57	1.34	0.98	7.3	0.92	7.1	1.37 [I]
2H-WS ₂ (194)	2.43	2.19	1.71	9.9	1.81	1.71	1.48	9.7	1.27	9.4	1.35 [I]
tet-SnO (129)	2.34	2.16	2.26	21.8	1.72	1.70	1.74	21.6	1.21	18.2	1.3 [I]
2H-MoS ₂ (194)	2.23	1.99	1.46	8.6	1.66	1.55	1.28	8.5	1.12	8.6	1.29 [I]
2H-WSe ₂ (194)	2.32	2.10	1.60	8.9	1.71	1.62	1.39	8.8	1.24	8.6	1.2 [I]
2H-MoSe ₂ (194)	2.18	1.95	1.38	7.8	1.57	1.47	1.20	7.6	1.10	7.8	1.10 [I]
1T-HfSe ₂ (164)	1.99	1.78	1.33	11.8	1.38	1.32	1.06	11.3	0.71	9.3	1.1 [I]
1T-SnSe ₂ (164)	2.19	1.85	1.48	13.4	1.56	1.38	1.15	12.8	0.86	10.7	0.98 [I]
2H-MoTe ₂ (194)	1.84	1.62	1.06	6.4	1.25	1.17	0.91	6.4	0.84	6.4	0.89 [I]
1T-TiS ₂ (164)	1.34	1.08	0.26	4.2	0.81	0.69	0.19	3.8	0.05	2.6	0.3 [I]
MAE (eV)	1.07	0.78	1.06	—	0.51	0.41	0.61	—	0.36	—	0
MAPE (%)	71.9	53.4	38.6	—	32.5	25.4	21.6	—	17.8	—	0
SD (eV)	0.44	0.44	1.31	—	0.43	0.44	1.00	—	0.53	—	0
linear fit slope	0.984	0.937	1.519	—	0.961	0.927	1.331	—	0.996	—	1
linear fit intercept	1.106	0.899	-0.239	—	0.528	0.447	-0.294	—	-0.103	—	0

of the results. This is clearly shown by the MAE of 1.03 eV for the band gap, which more than twice that with the standard B3LYP functional. Even larger is the MAPE (22.4%; **Table 2**). The intercept of the linear fit is -0.98, which clearly indicates the failure of this functional due to underestimation of band gap for some 3D metal oxides.

3.1.3. 3D Metal Oxides: Summary of DFT Results. The performances of the various functionals considered for the 24 3D metal oxides (**Table 2**) are summarized in a graphical way in **Figure 1**, where the theoretical band gaps are plotted against the experimental values. It emerges that the standard PBE0, HSE06, and B3LYP functionals exhibit better behavior and that the interpolation curves give trends closer to the experimental ones (**Table 2**). A general underestimate of the gap of large-gap insulators appears for all three functionals, but in general the trend is acceptable. We have seen before that the MAE is slightly better for B3LYP (0.46 eV) than for PBE0 (0.53 eV) and HSE06 (0.56 eV), although this could be partly fortuitous and related to the materials selected for the analysis.

The use of a DD functional, either global or range-separated, such as DD-B3LYP, DD-SC-BLYP, or DD-CAM-B3LYP, does not result in a systematic improvement of the results. It corrects some cases, but it also produces some systems where the prediction of the Kohn–Sham band gap is totally unreliable and physically incorrect.

On the basis of this analysis, we can conclude that *the use of the standard B3LYP, PBE0, and HSE06 functionals, while not perfect, offers a more homogeneous description of a wide series of 3D metal oxides*. This conclusion is consistent with a recent study by Garza and Scuseria, who found no significant statistical difference in the performance of PBE0, HSE06, and B3LYP for a wide group of semiconductors.¹¹⁴ Compared with dielectric-dependent functionals, these classical hybrid functionals have the additional advantage of not being material-dependent, which offers the possibility to treat doped systems, ternary and mixed oxides, and oxide heterojunctions more easily.¹¹⁵

In the next section, we will consider a different class of materials, layered or van der Waals crystalline solids, so-called quasi-2D materials, using the same set of functionals. We will show that there the situation is different and that in that case DD functionals, in particular the range-separated ones, may be useful for a better description of the band gap.

3.2. Quasi-2D Materials. In this section, we discuss the band gap properties of a series of 24 quasi-2D semiconductors, all having a layered structure with van der Waals forces acting among the layers. Actually, the present study stems from a critical case of two layered oxides, V₂O₅ and MoO₃, for which traditional exchange–correlation functionals fail to produce a good description of the electronic band gap and their direct or indirect nature.¹¹⁶ V₂O₅ and MoO₃ have similar band gaps (2.3

and 2.2 eV, respectively; **Table 5**), with absorption in the visible range. In both cases the gap is indirect, and a direct band gap of ~2.8 eV has been reported for both (see **Table 5**). Using three classical hybrid functionals, PBE0, B3LYP, and HSE06, one obtains indirect band gaps of 3.76, 3.31, and 3.12 eV for V_2O_5 and 4.10, 3.71, and 3.45 eV for MoO_3 , respectively (**Table 6**). In all cases, the predicted indirect-band-gap absorption is in the UV region, with errors of up to 70%. These results led us to consider DD functionals in order to see whether they would produce some improvement.

If we stay in the class of global hybrids and compare B3LYP with the DD version, DD-B3LYP, the results are discouraging. In fact, for V_2O_5 the gap goes from 3.31 to 3.57 eV, and for MoO_3 it goes from 3.71 to 4.05 eV (**Table 6**). In both cases, the use of a DD functional leads to larger errors. The situation is definitely better if we consider DD range-separated functionals (**Table 6**). For V_2O_5 , DD-SC-BLYP gives an indirect band gap of 2.81 eV; DD-CAM-B3LYP gives 2.48 eV, which is only slightly larger than the experimental value. Things are similar for MoO_3 (3.43 eV DD-SC-BLYP and 3.03 eV DD-CAM-B3LYP), although here the error remains large (but considerably smaller than with the classical functionals).

The question becomes the following: is this result specific to V_2O_5 and MoO_3 , or is it a general feature of bulk quasi-2D materials? To answer this question, we considered a series of 24 bulk structures based on the available experimental data on electronic band gaps and dielectric constants, including oxides, hydroxides, sulfides, selenides, etc.

3.2.1. Standard Hybrids: PBE0, B3LYP, HSE06, and SC-BLYP. The general performance of the PBE0 and B3LYP functionals for this series of 2D compounds is not particularly good. PBE0 has a MAE of 1.07 eV and a MAPE of 72%; B3LYP is slightly better, with a MAE of 0.78 eV and a MAPE of 53% (**Table 6**). The results are particularly poor for the small-gap materials, sulfides and selenides in particular. For $SnSe_2$, for instance, the experimental band gap is 0.98 eV, whereas PBE0 and B3LYP predict band gaps of 2.19 and 1.85 eV, respectively. TiS_2 , a material with very small band gap, 0.3 eV, is predicted to have a band gap of 1.34 eV (PBE0) or 1.08 eV (B3LYP). The other systems behave in a similar way. The situation is better for the large-gap quasi-2D semiconductors. Boron nitride, BN, is predicted to have a band gap of 6.58 eV (PBE0) or 6.18 eV (B3LYP), not too far from the experimental value of 5.96 eV (**Table 6**). In general, however, the performance of these two functionals is rather poor. This shows that while B3LYP and PBE0 work properly for 3D metal oxides (**Table 2**), they are not particularly accurate for layered compounds (**Table 6**).

The behavior of the range-separated functionals is much better. The critical case of $SnSe_2$ shows more realistic band gaps (1.56 eV HSE06 and 1.38 eV SC-BLYP vs 0.98 expt). TiS_2 has predicted band gaps of 0.81 and 0.69 eV with HSE06 and SC-BLYP, respectively, against 0.3 eV in experiment. For the large-gap quasi-2D materials, the performance is quite good, and the errors are in general small. For BN, for instance, the predictions are 5.85 and 5.64 eV for HSE06 and SC-BLYP, respectively, versus 5.96 eV in experiment (**Table 6**). This is reflected in better MAE and MAPE values: 0.51 and 33% for HSE06 and 0.41 and 25% for SC-BLYP, respectively. These results provide an indication that range-separated functionals are much better suited for the description of quasi-2D materials than PBE0 and B3LYP. Next, we consider the effect of using a DD functional.

3.2.2. Dielectric-Dependent Hybrids: DD-B3LYP, DD-SC-BLYP, and DD-CAM-B3LYP. In this section we consider the effect of using a DD functional, and we divide the discussion to consider first the global hybrid functional DD-B3LYP and then the range-separated functionals DD-SC-BLYP and DD-CAM-B3LYP.

A surprising result is that if we compare the MAEs for B3LYP and DD-B3LYP (**Table 6**), the error increases from 0.78 to 1.06 eV, respectively. Also, the SD values are 0.44 versus 1.31 eV, respectively. On the other hand, the MAPE of 53% for B3LYP decreases to 39% for DD-B3LYP. Such a contrast of MAE and MAPE for 30–40 binary semiconducting solids (containing four oxides, MgO , SiO_2 , ZnO , and $SrTiO_3$) has been discussed earlier.¹ We have already commented on the fact that for V_2O_5 and MoO_3 the use of a DD functional does not improve the results. This is true also for some large-gap materials such as BN, where the gap goes from 6.18 eV for B3LYP to 6.96 eV for DD-B3LYP (5.96 expt). On the other hand, there are some cases where there is a clear improvement. The gap in $SnSe_2$ decreases from 1.85 to 1.48 eV (0.98 expt); even better is the situation for TiS_2 , where a gap of 1.08 eV is predicted by B3LYP but DD-B3LYP predicts 0.26 eV, which is practically the experimental value (0.3 eV). Thus, there is an improvement for some materials, but this is not systematic and is accompanied by cases where the results are worse after use of a DD functional. The situation reflects what was found for the 3D metal oxides (see **Table 2**), where it was also shown that there is no general improvement with the use of a DD functional.

Now we consider the two DD range-separated functionals, DD-SC-BLYP and DD-CAM-B3LYP (**Table 6**). DD-SC-BLYP can be compared directly with the standard SC-BLYP version, with fixed $\alpha = 0.2$. In general, the behavior is similar, with a MAE that is slightly larger for the DD version (0.61 eV DD-SC-BLYP vs 0.41 eV SC-BLYP); on the other hand, the MAPE is smaller with the DD version (22% vs 25%). Also, the SD is larger (1.00 vs 0.44 eV, respectively). The two critical cases of V_2O_5 and MoO_3 do not show an improvement when the portion of exact exchange is obtained from the dielectric constant. For both oxides the gap is larger than in the experiment, and the difference with experiment increases with respect to the standard functionals. Also, for BN no clear improvement is observed, as the errors are similar with these two approaches, with SC-BLYP (5.64 eV) underestimating the experimental band gap (5.96 eV) and DD-SC-BLYP overestimating it (6.16 eV). On the other hand, a general improvement is found for the small-gap quasi-2D materials. Here the DD-SC-BLYP functional clearly performs relatively better than SC-BLYP. In $SnSe_2$ the gap goes from 1.38 to 1.15 eV, which is close to the experimental value of 0.98 eV. In TiS_2 , the values are 0.69 and 0.19 eV, respectively, again with the DD version showing a better agreement with the measured gap (0.3 eV) (**Table 6**).

The tendency of DD range-separated functionals to provide a satisfactory description of the quasi-2D materials is confirmed by the DD-CAM-B3LYP data (**Table 6**). All of the layered materials with band gaps below 3 eV are properly described by this functional. The two layered oxides where problems exist with other functionals are now described with sufficient accuracy: V_2O_5 has a gap of 2.48 eV (2.3 expt), and MoO_3 has a gap of 3.03 eV (2.2 expt). Some discrepancies are found for some large-gap quasi-2D materials, such as BN, for which a gap of 5.05 eV is predicted, which is 0.9 eV below the

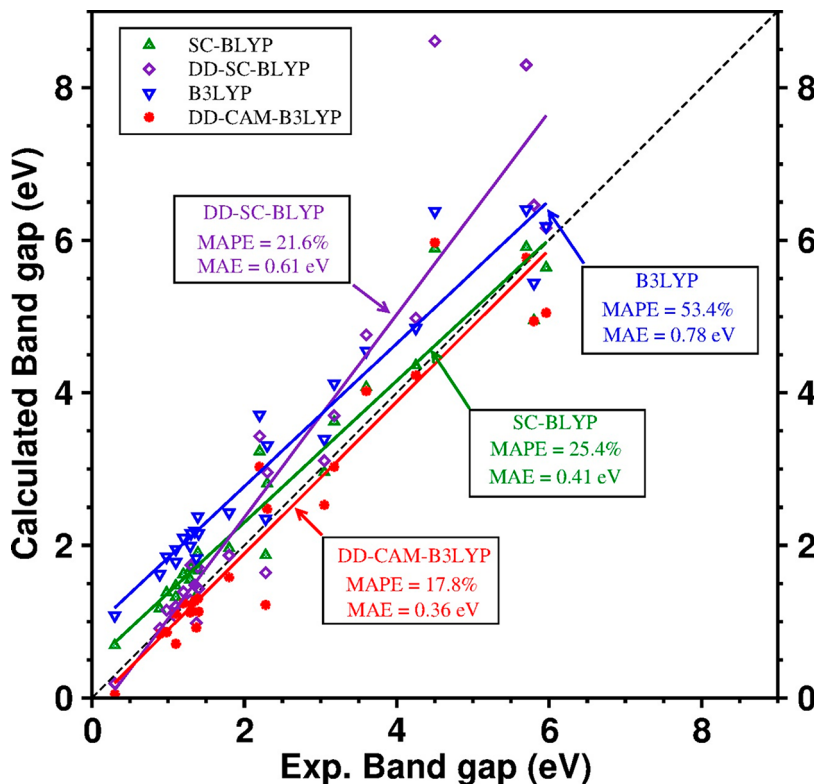


Figure 2. Correlations between computed and measured band gaps for the series of 24 quasi-2D materials (see Table 6).

experimental value. However, overall the MAE and MAPE for DD-CAM-B3LYP are 0.36 eV and 18%, respectively, which are the smallest values among all of the functionals considered (Table 6).

3.2.3. Quasi-2D Materials: Summary of DFT Results. From the data discussed above, one can draw two important conclusions: (1) range-separated functionals perform better than global hybrids for the description of the band gap of quasi-2D materials; (2) the use of DD functionals, contrary to the case of 3D metal oxides, does not worsen the results, and in some cases leads to a clear improvement. Unfortunately, this improvement is not systematic, and there are cases where the use of material-specific DD functionals results in less accurate gaps.

Some important consideration comes from the linear fits of the data in Figure 2 and Table 6 (plots of the band gaps from all seven functionals are given in Figure S2). The PBE0 and B3LYP curves have a slope close to 1 but an intercept of about 1 eV, indicating a systematic overestimation of the gap of the quasi-2D semiconductors. HSE06 has a similar slope, 0.96, and a considerably smaller intercept, 0.53 eV, showing the advantage of using a range-separated functional for these materials. When we consider the DD functionals, the only case where the linear fit shows a good behavior is that of DD-CAM-B3LYP: here the slope is almost exactly 1, and the intercept is close to zero (-0.10) (Table 6). The other two functionals considered, DD-B3LYP and DD-SC-BLYP, have wrong slopes (1.52 and 1.33, respectively), which reflect the fact that these functionals work better for small-gap quasi-2D semiconductors and fail for the large-gap solids. In both cases the intercept is relatively small (Table 6 and Figure 2).

To summarize, the description of quasi-2D materials requires range-separated functionals such as HSE06, and some of these functionals, in a DD version for the long-range

correction, can lead to a further improvement (this is the case of the DD-CAM-B3LYP functional). This is different from the case of 3D metal oxides, where no systematic improvement was found in using range-separated and DD functionals compared to standard global hybrids.

Before closing this section, we briefly discuss the performance of the various functionals in reproducing the dielectric constants of the quasi-2D materials. The experimentally determined dielectric constants for the 24 quasi-2D systems are given in Table 7, while the corresponding computed values are listed in Table 8. For most systems, the various functionals, standard or DD, give very similar dielectric constants. This is for instance the case with 2H-BN, 2H-GaS, SnS₂, MoS₂, MoSe₂, etc. On the other hand, for some materials there is a wide scattering of values. The most relevant case is probably TiS₂, with an experimental dielectric constant of 24 and computed values that range from 10.7 (PBE0) to 39.7 (DD-CAM-B3LYP) (Table 8). Another critical case is that of WS₂, for which the experimental value is 21.2 and all of the computed values are between 9.6 and 10.6. Not surprisingly, the DD functionals give smaller MAE and MAPE values, but these remain relatively large. The smallest MAE is found for DD-B3LYP, 2.22 eV, and the smallest MAPE for DD-CAM-B3LYP, 21.0%, but the values are similar for all three DD functionals considered. Also, it should be noted that for these 2D materials experimental dielectric constants are missing for six cases: Ca(OH)₂, BiOCl, BiOI, HfS₂, HfSe₂, and ReS₂.

4. PRINCIPAL COMPONENT ANALYSIS OF THE DFT RESULTS

Principal component analysis (PCA)^{29,30} can shed light on the most relevant factors influencing the calculation of the band gaps. The methodology has been successfully applied in recent

Table 7. Experimental Static Dielectric Constants, ϵ_{∞} , for the Series of 24 Quasi-2D Materials Considered in This Work^a

layered material (space group no.)	ϵ_{∞}	method
hexagonal 2H-MoS ₂ (194)	10.97	EELS on single crystal ¹⁶²
	12.3	reflectivity spectra ^{163–165}
	20.3	^b SE on films ¹⁶⁶
hexagonal 2H-MoSe ₂ (194)	14	reflectivity spectra ^{163,167}
	12.3	^c SE on films ¹⁶⁶
hexagonal 2H-MoTe ₂ (194)	16	reflectivity spectra ^{163,165}
hexagonal 2H-WS ₂ (194)	16	^d reflectance and KK transformation ¹⁶⁸
hexagonal 2H-WSe ₂ (194)	21.2	^e SE on films ¹⁶⁶
	20	reflectivity spectra and KK transformation ^{168,169}
	19.4	^c SE on films ¹⁶⁶
trigonal 1T-TiS ₂ (164)	24	^c vis-NIR spectra in SE ¹⁵⁹
trigonal CdCl ₂ (166)	3.0	EELS ¹¹⁸
trigonal CdI ₂ (164)	4.6	EELS ¹¹⁸
trigonal 1T-ZrS ₂ (164)	9.9	^c NIR-VIS spectra in SE ¹⁵⁹
trigonal Ca(OH) ₂ (164)	NA	—
trigonal Mg(OH) ₂ (164)	3.53	^e UV-vis spectroscopy ¹²²
tetragonal BiOCl (129)	NA	—
orthorhombic V ₂ O ₅ (59)	5.9	reflection measurement ¹⁷⁰
orthorhombic MoO ₃ (62)	5.7	refractive index measurement ¹⁷¹
tetragonal SnO (129)	NA	—
trigonal 1T-SnS ₂ (164)	6.93	IR-reflectance spectra, 300 K ¹⁷²
trigonal 1T-SnSe ₂ (164)	10.27	IR-reflectance spectra, 300 K ¹⁷²
trigonal 1T-HfS ₂ (164)	9.82	^f reflectivity spectra at 290 K ¹⁷³
	NA	—
	NA	—
hexagonal 2H-GaS (194)	5.86	infrared reflectivity ¹⁷⁴
hexagonal 2H-BN (194)	5.2	capacitance measurement ¹⁷⁵
	4.67	reflectance and transmission spectra ¹⁷⁶
triclinic 1T-ReS ₂ (2)	NA	—

^aAbbreviations: SE, spectroscopic ellipsometry; KK, Kramers-Kronig; NA, not available. ^bEstimated using the refractive index, n , at wavelength $\lambda = 1240$ nm using the $\epsilon_{\infty} = n^2$ relation. ^cIn-plane dielectric constant estimated from the real part of the dielectric function. ^dIn-plane dielectric constant estimated from the real part of the dielectric function at measurement wavelength $\lambda = 826.6$ nm. ^eDiffuse reflectance spectra (DRS) using a 1200 nm thick thin film at wavelengths of 300–2000 nm. ^fEstimated using the $\epsilon_{\infty} = n^2$ relation.

quantum-chemical studies.^{177,178} The aim is to identify the most significant observables describing a certain data set, as well as their reciprocal correlation, by applying a linear transformation on the data set. The transformed variables are called principal components (PCs), and their transformation coefficients are called loading vectors. A strong correlation between two variables corresponds to almost parallel loading vectors, while orthogonal or nearly orthogonal loading vectors indicate the absence of any significant correlation between the variables.

The analysis was performed using the R code¹⁷⁹ on both data sets described above (3D and quasi-2D structures), i.e., on the B3LYP, PBE0, SC-BLYP, HSE06, DD-B3LYP, DD-SC-BLYP, and DD-CAM-B3LYP results. In Figure 3a–d we report results concerning the PBE0, B3LYP, SC-BLYP, and HSE06 data sets. The variables included in the analysis (reported as loading vectors) are the deviation from the experimental gap (E_g^{err}), the corresponding percentage deviation (% E_g^{err}), the

average metal–nonmetal (M–X) distance, the periods of the metal atom and nonmetal atom in the periodic table, the 3D or van der Waals (VDW) nature of the material, and the ionicity index, defined as the deviation of the anion's Mulliken charge from the formal charge (−2 for O, S, Se, and Te and −3 for N). Such an index, even though not quantitative, can be used as a descriptor of the material's ionicity. The reliability of the analysis was checked by adding two control cases, namely, variables whose reciprocal correlation is known. When possible, we have added the calculated static dielectric constant and the exact exchange fraction used in the calculation of each oxide. We already know that we used $\alpha = \frac{1}{\epsilon_{\infty}}$ for the DD-B3LYP, DD-SC-BLYP, and DD-CAM-B3LYP calculations, and thus, we should find the two variables in the plots to be anticorrelated, i.e., with a reciprocal angle close to 180°. The variables in the loadings plot are reported in the reference frame of the two most relevant principal components, PC1 and PC2, as assessed by Colombo et al.¹⁷⁸

Figure 3a and Figure 3b display very similar pictures, indicating some similarities between B3LYP and PBE0 in the band gap estimate accuracy, as is also clear from Table 2. The error in the calculated band gap, E_g^{err} , is anticorrelated (angle close to 180°) with the ionic nature of the oxide, i.e., we find worse performances for more covalent oxides. This can be also appreciated quantitatively by looking at Figure S3. The % E_g^{err} and E_g^{err} are correlated with the layered nature of the oxides (labeled as VDW), as is also evident from Table 6. Indeed, when we evaluate the MAE between calculated and experimental gaps only for quasi-2D layered materials, it becomes 0.78 and 1.07 eV for B3LYP and PBE0, respectively. If we instead restrict the calculation to the 3D metal oxides (nonlayered ones), the deviation decreases significantly to 0.46 and 0.53 eV for B3LYP and PBE0, respectively. As suggested also by PCA, the % E_g^{err} is even more sensitive to the nature of the material. Indeed, the MAPEs with B3LYP and PBE0 are 53% and 72%, respectively, for quasi-2D materials, and they strongly decrease to 10% and 13% when only 3D materials are considered.

On the opposite side, the SC-BLYP and HSE06 functionals seem to show a more general robustness over the range of materials considered since no significant correlations between the error and the other variables such as the layered nature, the location in the periodic table, or the ionicity are found (Figure 3c,d). Indeed, the two functionals work sufficiently well for both 3D and 2D materials, since the MAEs and MAPEs are comparable to those of B3LYP and PBE0 for 3D materials and are significantly lower for the quasi-2D class.

Figure 4a–c reports results arising from the DD-SC-BLYP, DD-B3LYP, and DD-CAM-B3LYP functionals, respectively. We first observe that our control case leads to the expected result, i.e., the calculated dielectric constant and the exact exchange are almost perfectly counter-correlated.

The picture of DD-SC-BLYP is analogous to that of SC-BLYP, in analogy to what was previously discussed. In DD-B3LYP, the optimization of α attenuates the correlation between the accuracy of the band gap and the 2D nature of the material under examination compared with the B3LYP results. Indeed, the MAEs are now very similar for the 2D layered and 3D nonlayered materials (1.06 and 1.25 eV, respectively). As for DD-SC-BLYP, Figure 4a indicates a strong correlation of E_g^{err} with α , i.e., smaller errors are found for cases where α is small. In the case of DD-CAM-B3LYP, a significant counter-

Table 8. Dielectric Constants Computed with Different Functionals for the Series of 24 Quasi-2D Materials (For Experimental Data, Also See Table 7)

layered material (space group no.)	global hybrid			range-separated hybrid			expt
	PBE0 ($\alpha = 25\%$)	B3LYP ($\alpha = 20\%$)	DD-B3LYP	SC-BLYP ($\alpha = 20\%$)	DD-SC-BLYP	DD-CAM-B3LYP	
2H-BN (194)	3.53	3.56	3.45	3.57	3.46	4.04	4.67
1T-CdCl ₂ (166)	2.34	2.39	2.22	2.39	2.22	2.62	3.0
1T-Mg(OH) ₂ (164)	2.17	2.17	2.03	2.17	2.02	2.36	3.53
1T-Ca(OH) ₂ (164)	1.89	1.90	1.77	1.97	1.82	2.02	NA
l-TiO ₂ (63)	3.50	3.60	3.42	3.63	3.45	3.86	NA
1T-CdI ₂ (164)	2.90	2.96	2.81	2.97	2.82	3.25	4.6
tet-BiOCl (129)	4.53	4.55	4.50	4.59	4.54	5.32	NA
2H-GaS (194)	4.18	4.26	4.21	4.29	4.24	4.82	5.2
α -V ₂ O ₅ (59)	4.27	4.44	4.43	4.52	4.45	4.89	5.9
1T-SnS ₂ (164)	6.39	6.62	6.91	6.81	7.10	8.48	6.93
α -MoO ₃ (62)	4.10	4.20	4.10	4.27	4.19	4.65	5.7
tet-BiOI (129)	5.76	5.82	5.93	5.91	6.03	6.87	NA
1T-ZrS ₂ (164)	6.75	6.98	7.47	7.24	7.74	9.23	9.9
1T-HfS ₂ (164)	6.18	6.34	6.61	6.49	6.76	8.22	NA
3R-ReS ₂ (2)	10.94	11.92	13.23	12.53	13.69	14.16	NA
2H-WS ₂ (194)	9.60	9.84	10.16	10.02	10.27	10.59	21.2
tet-SnO (129)	4.59	4.62	4.58	4.67	4.63	5.48	NA
2H-MoS ₂ (194)	10.9	11.23	11.58	11.54	11.78	11.68	12.3
2H-WSe ₂ (194)	10.5	10.80	11.25	11.05	11.40	11.66	19.4
2H-MoSe ₂ (194)	12.1	12.47	12.89	12.86	13.13	12.84	14
1T-HfSe ₂ (164)	7.40	7.68	8.51	8.02	8.84	10.80	NA
1T-SnSe ₂ (164)	6.65	7.03	7.50	7.35	7.84	9.31	9.82
2H-MoTe ₂ (194)	14.6	15.03	15.78	15.66	16.13	15.74	16
1T-TiS ₂ (164)	10.7	11.9	24.10	13.73	26.90	39.65	24
MAE	3.40	3.14	2.22	2.86	2.30	2.80	0
MAPE (%)	28.7	26.5	22.7	24.5	22.7	21.0	0

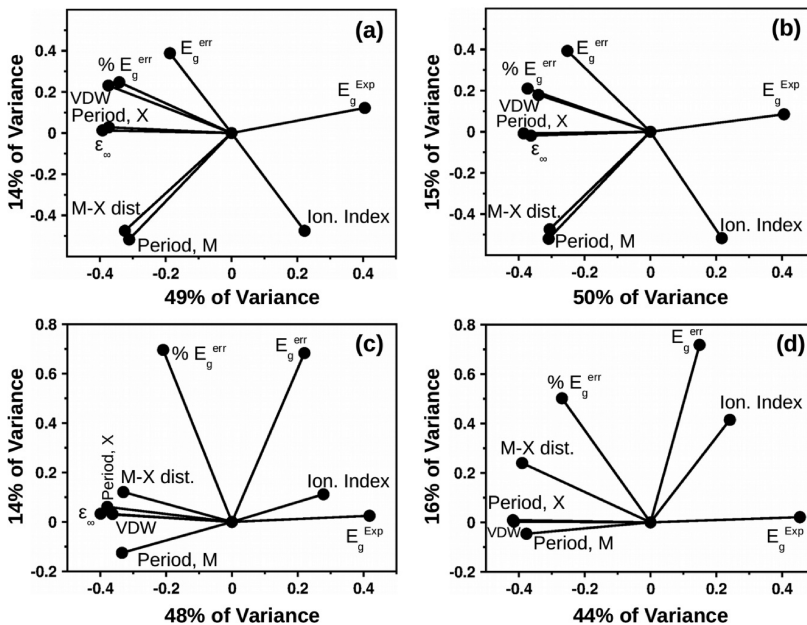


Figure 3. Loading plots for (a) B3LYP, (b) PBE0, (c) SC-BLYP, and (d) HSE06 data. Variables are reported with black lines in the reference frame defined by the first two principal components (PC1 along the *x* axis, PC2 along the *y* axis), with the contributions to the total variance reported.

correlation (152°) between the error and layered nature of the oxide is reported, similarly to what happens with the other range-separated functionals. Also, in this case the functional seems to be suitable for layered oxides, since the MAE is very small, only 0.36 eV, to be compared with the overall accuracy of 1.03 eV for 3D metal oxides.

5. CONCLUSIONS

In this study we have compared the performances of various hybrid functionals with the scope to analyze their performance in the description of the Kohn–Sham band gaps of a wide series of metal oxides with 3D structure and quasi-2D inorganic materials (oxides, hydroxides, sulfides, etc.) with

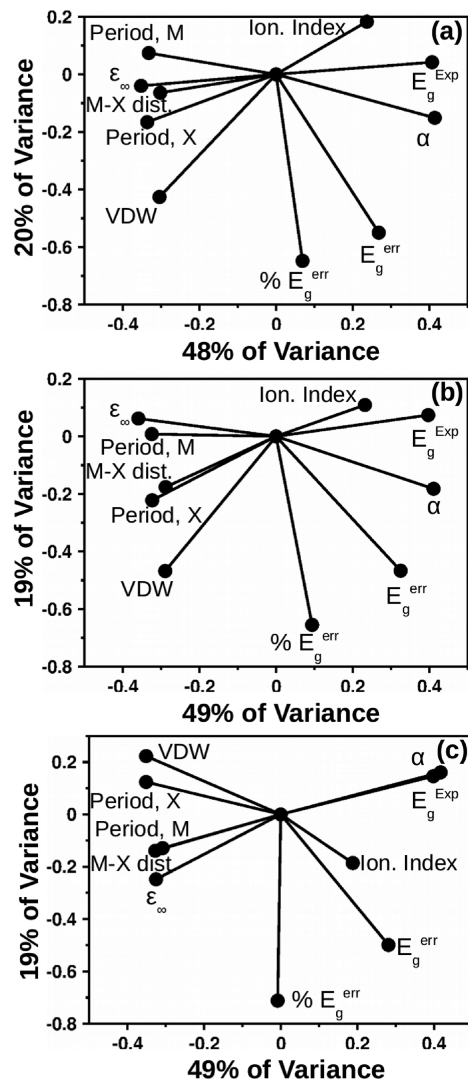


Figure 4. Loading plots for (a) DD-SC-BLYP, (b) DD-B3LYP, and (c) DD-CAM-B3LYP data. Variables are reported with black lines in the reference frame defined by the first two principal components (PC1 along the *x* axis, PC2 along the *y* axis), with the contributions to the total variance reported.

band gaps ranging from about 0 to about 11 eV. The work was stimulated by the finding that the standard hybrid functionals B3LYP, PBE0, and HSE06 fail in properly describing the band gap in some specific quasi-2D layered oxides, MoO_3 and V_2O_5 in particular. To this end, besides these functionals, we also considered some dielectric-dependent (DD) functionals, where the portion of exact exchange has been determined self-consistently for each of the 24 3D metal oxides and 24 quasi-2D materials considered. All of the calculations were performed with the CRYSTAL17 code, and the choice of the functionals used was partly dictated by the availability of the functional implemented in this version of the code. We computed the Kohn–Sham band gaps of the 48 systems using three global hybrid functionals and four range-separated hybrid functionals. These in turn were divided into standard functionals (PBE0, B3LYP, HSE06, and SC-BLYP) and dielectric-dependent functionals (DD-B3LYP, DD-SC-BLYP, and DD-CAM-B3LYP).

The first surprising result is that the use of DD functionals, either global or range-separated, does not really lead to a

general improvement of the band gap of the 3D metal oxides. While in a few cases some improvement is found, on average the description of most of the oxides deteriorates when DD functionals are used. The analysis of the mean absolute errors gives the surprising result not only that the classical hybrid functionals B3LYP, PBE0, and HSE06 perform better for the group of oxides considered but also that B3LYP gives the smallest absolute error.

On the other hand, range-separated functionals such as HSE06 work better for the quasi-2D materials, and some of these functionals, in a DD version, can lead to a further improvement (this is the case for the DD-CAM-B3LYP functional). At this level of theory, even the critical MoO_3 and, in particular, V_2O_5 layered oxides are described with acceptable accuracy. It thus appears that the screening, in particular in the long-range part, is crucial to yield a good description of the band gap in layered materials. This intuitively matches with the nature of these structures, where long-range interactions between separated layers play a relevant role. However, we cannot go beyond a phenomenological interpretation of this fact at this stage.

It has recently been reported¹⁸⁰ that the role of double screening parameters from the dielectric function and metallic screening for solids is important. However, this has not been specifically applied to the metal oxides and quasi-2D materials considered in this work. This needs to be further investigated in future research work.

These conclusions are corroborated by principal component analysis, which indicated that PBE0 and B3LYP display common properties, both being more suitable for 3D oxides with an ionic nature and large gap. In particular, the error in the calculated band gap is positively correlated with the layered nature of the material. The range-separated HSE06 and SC-BLYP functionals are generally robust, regardless of the 3D or 2D nature of the material. In the case of DD-CAM-B3LYP, the error in the band gaps is counter-correlated with the 2D nature of the material, i.e., this functional looks particularly suitable for layered van der Waals inorganic solids.

ASSOCIATED CONTENT

S Supporting Information

The Supporting Information is available free of charge on the ACS Publications website at DOI: 10.1021/acs.jctc.9b00545.

List of basis sets used (Table S1); calculated band gaps of 3D oxides versus experiment for all functionals (Figure S1); experimental lattice constants for the 48 materials considered (Table S2); calculated band gaps of quasi-2D materials versus experiment for all functionals (Figure S2); effect of lattice relaxation on the band gap (Table S3) (PDF)

AUTHOR INFORMATION

Corresponding Author

*E-mail: gianfranco.pacchioni@unimib.it.

ORCID

Giovanni Di Liberto: 0000-0003-4289-2732

Sergio Tosoni: 0000-0001-5700-4086

Gianfranco Pacchioni: 0000-0002-4749-0751

Funding

Financial support from the Italian Ministry of University and Research (MIUR) through the PRIN Project 2015K7FZLH

SMARTNESS “Solar driven chemistry: new materials for photo- and electro-catalysis” and the grant Dipartimenti di Eccellenza - 2017 “Materials for Energy” is gratefully acknowledged. Access to the CINECA supercomputing resources was granted via the ISCRA initiative.

Notes

The authors declare no competing financial interest.

■ REFERENCES

- (1) Civalleri, B.; Presti, D.; Dovesi, R.; Savin, A. On choosing the best density functional approximation. *Chem. Model.* **2012**, *9*, 168–185.
- (2) He, J.; Franchini, C. Assessing the performance of self-consistent hybrid functional for band gap calculation in oxide semiconductors. *J. Phys.: Condens. Matter* **2017**, *29*, 454004.
- (3) Gerosa, M.; Bottani, C. E.; Di Valentin, C.; Onida, G.; Pacchioni, G. Accuracy of dielectric-dependent hybrid functionals in the prediction of optoelectronic properties of metal oxide semiconductors: a comprehensive comparison with many-body GW and experiments. *J. Phys.: Condens. Matter* **2018**, *30*, No. 044003.
- (4) Heyd, J.; Peralta, J. E.; Scuseria, G. E.; Martin, R. L. Energy band gaps and lattice parameters evaluated with the Heyd-Scuseria-Ernzerhof screened hybrid functional. *J. Chem. Phys.* **2005**, *123*, 174101.
- (5) Tran, F.; Blaha, P. Importance of the kinetic energy density for band gap calculations in solids with density functional theory. *J. Phys. Chem. A* **2017**, *121*, 3318–3325.
- (6) Borlido, P.; Aull, T.; Huran, A. W.; Tran, F.; Marques, M. A. L.; Botti, S. Large scale benchmark of exchange-correlation functionals for the determination of electronic band gaps of solids. *J. Chem. Theory Comput.* **2019**, *15*, 5069–5079.
- (7) Perdew, J. P.; et al. Understanding band gaps of solids from generalized Kohn–Sham theory. *Proc. Natl. Acad. Sci. U. S. A.* **2017**, *114* (11), 2801–2806.
- (8) Muscat, J.; Wander, A.; Harrison, N. M. On the prediction of band gaps from hybrid functional theory. *Chem. Phys. Lett.* **2001**, *342*, 397–401.
- (9) Corà, F.; Alfredsson, M.; Mallia, G.; Middlemiss, D. S.; Mackrodt, W. C.; Dovesi, R.; Orlando, R. The performance of hybrid density functionals in solid state chemistry. In *Principles and Applications of Density Functional Theory in Inorganic Chemistry II*; Springer: Berlin, 2004; pp 171–232.
- (10) Marsman, M.; Paier, J.; Stroppa, A.; Kresse, G. Hybrid functionals applied to extended systems. *J. Phys.: Condens. Matter* **2008**, *20*, No. 064201.
- (11) Erba, A.; Baima, J.; Bush, I.; Orlando, R.; Dovesi, R. Large-scale condensed matter DFT simulations: performance and capabilities of the CRYSTAL code. *J. Chem. Theory Comput.* **2017**, *13*, 5019–5027.
- (12) Paier, J.; Marsman, M.; Hummer, K.; Kresse, G.; Gerber, I. C.; Ángyán, J. G. Screened hybrid density functionals applied to solids. *J. Chem. Phys.* **2006**, *124*, 154709.
- (13) Cohen, A. J.; Mori-Sánchez, P.; Yang, W. Challenges for density functional theory. *Chem. Rev.* **2012**, *112*, 289–320 and references therein.
- (14) Stephens, P. J.; Devlin, F. J.; Chabalowski, C.; Frisch, M. J. Ab initio calculation of vibrational absorption and circular dichroism spectra using density functional force fields. *J. Phys. Chem.* **1994**, *98*, 11623–11627.
- (15) Adamo, C.; Barone, V. Toward reliable density functional methods without adjustable parameters: The PBE0 model. *J. Chem. Phys.* **1999**, *110*, 6158.
- (16) Perdew, J. P.; Ernzerhof, M.; Burke, K. Rationale for mixing exact exchange with density functional approximations. *J. Chem. Phys.* **1996**, *105*, 9982–9985.
- (17) Moreira, I. d. P. R.; Illas, F.; Martin, R. L. Effect of Fock exchange on the electronic structure and magnetic coupling in NiO. *Phys. Rev. B: Condens. Matter Mater. Phys.* **2002**, *65*, 155102.
- (18) Da Silva, J. L.; Ganduglia-Pirovano, M. V.; Sauer, J.; Bayer, V.; Kresse, G. Hybrid functionals applied to rare-earth oxides: The example of ceria. *Phys. Rev. B: Condens. Matter Mater. Phys.* **2007**, *75*, No. 045121.
- (19) Tran, F.; Blaha, P.; Schwarz, K.; Novák, P. Hybrid exchange-correlation energy functionals for strongly correlated electrons: Applications to transition-metal monoxides. *Phys. Rev. B: Condens. Matter Mater. Phys.* **2006**, *74*, 155108.
- (20) Engel, E.; Schmid, R. N. Insulating ground states of transition-metal monoxides from exact exchange. *Phys. Rev. Lett.* **2009**, *103*, No. 036404.
- (21) Heyd, J.; Scuseria, G. E.; Ernzerhof, M. Hybrid functionals based on a screened Coulomb potential. *J. Chem. Phys.* **2003**, *118*, 8207–8215.
- (22) Schimka, L.; Harl, J.; Kresse, G. Improved hybrid functional for solids: The HSE06sol functional. *J. Chem. Phys.* **2011**, *134*, No. 024116.
- (23) Hinuma, Y.; Kumagai, Y.; Tanaka, I.; Oba, F. Band alignment of semiconductors and insulators using dielectric-dependent hybrid functionals: Toward high-throughput evaluation. *Phys. Rev. B: Condens. Matter Mater. Phys.* **2017**, *95*, No. 075302.
- (24) Shimazaki, T.; Asai, Y. Band structure calculations based on screened Fock exchange method. *Chem. Phys. Lett.* **2008**, *466*, 91–94.
- (25) Alkauskas, A.; Broqvist, P.; Pasquarello, A. Defect levels through hybrid density functionals: insights and applications. *Phys. Status Solidi B* **2011**, *248*, 775–789.
- (26) Skone, J. H.; Govoni, M.; Galli, G. Self-consistent hybrid functional for condensed systems. *Phys. Rev. B: Condens. Matter Mater. Phys.* **2014**, *89*, 195112.
- (27) Chen, W.; Miceli, G.; Rignanese, G. M.; Pasquarello, A. Nonempirical dielectric-dependent hybrid functional with range separation for semiconductors and insulators. *Phys. Rev. Mater.* **2018**, *2*, No. 073803.
- (28) Jana, S.; Samal, P. A meta-GGA level screened range-separated hybrid functional by employing short range Hartree-Fock with a long range semilocal functional. *Phys. Chem. Chem. Phys.* **2018**, *20*, 8999.
- (29) Jolliffe, I. T. *Principal Component Analysis*, 2nd ed.; Springer Series in Statistics; Springer: New York, 2002.
- (30) Beebe, K. R.; Pell, R. J.; Seasholtz, M. B. *Chemometrics: A Practical Guide*; Wiley-Interscience: New York, 1998.
- (31) Ferrero, M.; Rérat, M.; Orlando, R.; Dovesi, R. The calculation of static polarizabilities of 1–3D periodic compounds. The implementation in crystal code. *J. Comput. Chem.* **2008**, *29*, 1450–1459.
- (32) Ferrero, M.; Rérat, M.; Orlando, R.; Dovesi, R. Coupled perturbed Hartree-Fock for periodic systems: the role of symmetry and related computational aspects. *J. Chem. Phys.* **2008**, *128*, No. 014110.
- (33) Ferrero, M.; Rérat, M.; Kirtman, B.; Dovesi, R. Calculation of first and second static hyperpolarizabilities of one- to three-dimensional periodic compounds. Implementation in CRYSTAL Code. *J. Chem. Phys.* **2008**, *129*, 244110.
- (34) Dovesi, R.; Orlando, R.; Erba, R.; Zicovich-Wilson, C. M.; Civalleri, B.; Casassa, S.; Maschio, L.; Ferrabone, M.; de la Pierre, M.; D’Arco, P.; Noel, Y.; Causa, M.; Rerat, M.; Kirtman, B. *Int. J. Quantum Chem.* **2014**, *114*, 1287–1317.
- (35) Peintinger, M. F.; Oliveira, D. V.; Bredow, T. Consistent Gaussian basis sets of triple-zeta valence with polarization quality for solid state calculations. *J. Comput. Chem.* **2013**, *34*, 451–459.
- (36) Tawada, Y.; Tsuneda, T.; Yanagisawa, S.; Yanai, T.; Hirao, K. A long-range-corrected time-dependent density functional theory. *J. Chem. Phys.* **2004**, *120*, 8425–8433.
- (37) Yanai, T.; Tew, D. P.; Handy, N. C. A new hybrid exchange-correlation functional using the Coulomb-Attenuating method (CAM-B3LYP). *Chem. Phys. Lett.* **2004**, *393*, 51–57.
- (38) Gerber, I. C.; Ángyán, J. G. Hybrid functional with separated range. *Chem. Phys. Lett.* **2005**, *415*, 100–105.
- (39) Chioldo, L.; García-Lastra, J. M.; Iacomino, A.; Ossicini, S.; Zhao, J.; Petek, H.; Rubio, A. Self-energy and excitonic effects in the

- electronic and optical properties of TiO_2 crystalline phases. *Phys. Rev. B: Condens. Matter Mater. Phys.* **2010**, *82*, No. 045207.
- (40) Laskowski, R.; Christensen, N. E.; Blaha, P.; Palanivel, B. Strong excitonic effects in CuAlO_2 delafossite transparent conductive oxides. *Phys. Rev. B: Condens. Matter Mater. Phys.* **2009**, *79*, 165209.
- (41) Roessler, D. M.; Walker, W. C.; Loh, E. Electronic spectrum of crystalline beryllium oxide. *J. Phys. Chem. Solids* **1969**, *30*, 157–167.
- (42) Cline, C. F.; Kahn, J. S. Microhardness of single crystals of BeO and other wurtzite compounds. *J. Electrochem. Soc.* **1963**, *110*, 773.
- (43) Godmanis, I. T.; Trukhin, A. N.; Hübner, K. Exciton and phonon interaction in crystalline and vitreous SiO_2 . *Phys. Status Solidi B* **1983**, *116*, 279.
- (44) Wemple, S. H. Refractive-index behaviour in amorphous semiconductors and glasses. *Phys. Rev. B* **1973**, *7*, 3767.
- (45) Innocenzi, M. E.; Swimm, R. T.; Bass, M.; French, R. H.; Villaverde, A. B.; Kokta, M. R. Room temperature optical absorption in undoped $\alpha\text{-Al}_2\text{O}_3$. *J. Appl. Phys.* **1990**, *67*, 7542.
- (46) Arakawa, E. T.; Williams, M. W. Optical properties of aluminum oxide in the vacuum ultraviolet. *J. Phys. Chem. Solids* **1968**, *29*, 735–744.
- (47) Wemple, S. H.; Pinnow, D. A.; Rich, T. C.; Jaeger, R. E.; Van Uitert, L. G. Binary $\text{SiO}_2\text{-B}_2\text{O}_3$ glass system: Refractive index behavior and energy gap consideration. *J. Appl. Phys.* **1973**, *44*, 5432.
- (48) Terashima, K.; Uchino, T.; Hashimoto, T.; Yoko, T. Structure and nonlinear optical properties of $\text{BaO}\text{-TiO}_2\text{-B}_2\text{O}_3$ glasses. *Nippon Seramikkusu Kyokai Gakujutsu Ronbunshi* **1997**, *105*, 288–293.
- (49) Suzuki, T.; Hirano, M.; Hosono, H. Optical gaps of alkali borate and alkali fluoroborate glasses. *J. Appl. Phys.* **2002**, *91*, 4149–4153.
- (50) Ishii, Y.; Murakami, J.-i.; Itoh, M. Optical spectra of excitons in lithium oxide. *J. Phys. Soc. Jpn.* **1999**, *68*, 696.
- (51) Albrecht, S.; Onida, G.; Reining, L. Ab-initio calculations of the quasiparticle spectrum and excitonic effect in Li_2O . *Phys. Rev. B: Condens. Matter Mater. Phys.* **1997**, *55*, 10278–10281.
- (52) Whited, R. C.; Flaten, C. J.; Walker, W. C. Exciton thermorelectance of MgO and CaO . *Solid State Commun.* **1973**, *13*, 1903–1905.
- (53) Emeline, A. V.; Kataeva, G. V.; Ryabchuk, V. K.; Serpone, N. Photosimulated generation of defects and surface reactions on a series of wide band gap metal-oxide solids. *J. Phys. Chem. B* **1999**, *103*, 9190–9199.
- (54) Reiling, G. H.; Hensley, E. B. Fundamental optical absorption in magnesium oxide. *Phys. Rev.* **1958**, *112*, 1106.
- (55) Neeley, V. I.; Kemp, J. C. Optical absorption in CaO single crystals. *J. Phys. Chem. Solids* **1963**, *24*, 1301–1304.
- (56) Rao, A. S.; Kearney, R. J. Logarithmic derivative reflectance spectra of BaO and SrO . *Phys. Status Solidi B* **1979**, *95*, 243.
- (57) French, R. H.; Glass, S. J.; Ohuchi, F. S.; Xu, Y. N.; Ching, W. Y. Experimental and theoretical determination of the electronic structure and optical properties of three phases of ZrO_2 . *Phys. Rev. B: Condens. Matter Mater. Phys.* **1994**, *49*, 5133.
- (58) Dash, L. K.; Vast, N.; Baranek, P.; Cheynet, M.-C.; Reining, L. Electronic structure and electron energy-loss spectroscopy of ZrO_2 zirconia. *Phys. Rev. B: Condens. Matter Mater. Phys.* **2004**, *70*, 245116.
- (59) Balog, M.; Schieber, M.; Michman, M.; Patai, S. Chemical vapor deposition and characterization of hafnium oxide films from organo-hafnium compounds. *Thin Solid Films* **1977**, *41*, 247–259.
- (60) He, G.; Zhu, L. Q.; Liu, M.; Fang, Q.; Zhang, L. D. Optical and electrical properties of plasma-oxidation derived HfO_2 gate dielectric films. *Appl. Surf. Sci.* **2007**, *253*, 3413–3418.
- (61) Madelung, O. *Semiconductors: Data Handbook*, 3rd ed.; Springer: Berlin, 2004; p 593.
- (62) Rauch, W. Die ultravioletten Dispersionsfrequenzen der Alkalioxide. *Eur. Phys. J. A* **1940**, *116*, 652.
- (63) Onuma, T.; Saito, S.; Sasaki, K.; Masui, T.; Yamaguchi, T.; Honda, T.; Higashiwaki, M. Valence band ordering in $\beta\text{-Ga}_2\text{O}_3$ studied by polarized transmittance and reflectance spectroscopy. *Jpn. J. Appl. Phys.* **2015**, *54*, 112601.
- (64) Zollweg, R. J. Optical absorption and photoemission of barium and strontium oxides, sulfides, selenides, and tellurides. *Phys. Rev.* **1958**, *111*, 113.
- (65) Saum, G. A.; Hensley, E. B. Fundamental optical absorption in the IIA-VIB compounds. *Phys. Rev.* **1959**, *113*, 1019.
- (66) Janowitz, C.; et al. Experimental electronic structure of In_2O_3 and Ga_2O_3 . *New J. Phys.* **2011**, *13*, No. 085014.
- (67) Weiher, R. L.; Ley, R. P. Optical properties of Indium oxide. *J. Appl. Phys.* **1966**, *37*, 299.
- (68) Reimann, K.; Steube, M. Experimental determination of the electronic band structure of SnO_2 . *Solid State Commun.* **1998**, *105*, 649–652.
- (69) Nagasawa, M.; Shionoya, S. Urbach's rule is exhibited in SnO_2 . *Solid State Commun.* **1969**, *7*, 1731–1733.
- (70) Kawasaki, B. S.; Garside, B. K.; Shewchun, J. Electron beam luminescence of SnO_2 . *Proc. IEEE* **1970**, *58*, 179.
- (71) Liang, W. Y.; Yoffe, A. D. Transmission spectra of ZnO single crystal. *Phys. Rev. Lett.* **1968**, *20*, 59.
- (72) Reynolds, D. C.; Look, D. C.; Jogai, B.; Litton, C. W.; Cantwell, G.; Harsch, W. C. *Phys. Rev. B: Condens. Matter Mater. Phys.* **1999**, *60*, 2340.
- (73) Srikant, V.; Clarke, D. R. On the optical band gap of zinc oxide. *J. Appl. Phys.* **1998**, *83*, 5447.
- (74) Meyer, J.; Kroger, M.; Hamwi, S.; Gnam, F.; Riedl, T.; Kowalsky, W.; Kahn, A. Charge generation layers comprising transition metal-oxide/organic interfaces: Electronic structure and charge generation mechanism. *Appl. Phys. Lett.* **2010**, *96*, 193302.
- (75) Koffyberg, F. P.; Dwight, K.; Wold, A. Interband transition of semiconducting oxides determined from photoelectrolysis spectra. *Solid State Commun.* **1979**, *30*, 433–437.
- (76) van Benthem, K.; Elsässer, C.; French, R. H. Bulk electronic structure of SrTiO_3 : Experiment and theory. *J. Appl. Phys.* **2001**, *90*, 6156.
- (77) Goubin, F.; Rocquefelte, X.; Whangbo, M.-H.; Montardi, Y.; Brec, R.; Jobic, S. Experimental and theoretical characterization of the optical properties of CeO_2 , SrCeO_3 and Sr_2CeO_4 containing Ce^{4+} (f^0) ions. *Chem. Mater.* **2004**, *16*, 662–669.
- (78) Guo, S.; Arwin, H.; Jacobsen, S.; Järrendahl, K.; Helmersson, U. A spectroscopic ellipsometry study of cerium dioxide thin films grown on sapphire by rf magnetron sputtering. *J. Appl. Phys.* **1995**, *77*, 5369.
- (79) Scanlon, D. O.; et al. Band alignment of rutile and anatase TiO_2 . *Nat. Mater.* **2013**, *12*, 798.
- (80) Tang, H.; Levy, F.; Berger, H.; Schmid, P. E. Urbach tail of anatase TiO_2 . *Phys. Rev. B: Condens. Matter Mater. Phys.* **1995**, *52*, 7771.
- (81) Pascual, J.; Camassel, J.; Mathieu, H. Fine structure in the intrinsic absorption edge of TiO_2 . *Phys. Rev. B: Condens. Matter Mater. Phys.* **1978**, *18*, 5606.
- (82) Cooper, J. K.; Gul, S.; Toma, F. M.; Chen, L.; Liu, Y.-S.; Guo, J.; Ager, J. W.; Yano, J.; Sharp, I. D. Indirect bandgap and optical properties of bismuth vanadate. *J. Phys. Chem. C* **2015**, *119*, 2969.
- (83) Stoltzfus, M. W.; Woodward, P. K.; Seshadri, R.; Klepeis, J.-H.; Bursten, B. Structure and bonding in SnWO_4 , PbWO_4 and BiVO_4 : Lone pairs vs. inert pairs. *Inorg. Chem.* **2007**, *46*, 3839–3850.
- (84) Wang, Y.; Miska, P.; Pilloud, D.; Horwat, D.; Mücklich, F.; Pierson, J. F. Transmittance enhancement and optical band gap widening of Cu_2O thin films after air annealing. *J. Appl. Phys.* **2014**, *115*, No. 073505.
- (85) Jolk, A.; Klingshirn, C. F. Linear and nonlinear excitonic absorption and photoluminescence spectra in Cu_2O : Line shape analysis and exciton drift. *Phys. Status Solidi B* **1998**, *206*, 841.
- (86) Wang, Y.; Lany, S.; Ghanbaja, J.; Fagot-Revurat, Y.; Chen, Y. P.; Soldera, F.; Horwat, D.; Mücklich, F.; Pierson, J. F. Electronic structure of Cu_2O , Cu_4O_3 and CuO : A joint experimental and theoretical study. *Phys. Rev. B: Condens. Matter Mater. Phys.* **2016**, *94*, 245418.
- (87) Kim, T. A.; Ping, Y.; Galli, G. A.; Choi, K.-S. Simultaneous enhancements of photon absorption and charge transport of bismuth

- vanadate photoanodes for solar water splitting. *Nat. Commun.* **2015**, *6*, 8769.
- (88) Madelung, O. *Semiconductors: Data Handbook*, 3rd ed.; Springer: Berlin, 2004; pp 180–181.
- (89) Malyi, O. I.; Boström, M.; Kulish, V. V.; Thiyyam, P.; Parsons, D. F.; Persson, C. Volume dependence of the dielectric properties of amorphous SiO₂. *Phys. Chem. Chem. Phys.* **2016**, *18*, 7483–7489.
- (90) Philipp, H. R. *Handbook of Optical Constants of Solids*; Palik, E. D., Ed.; Academic Press: San Diego, 1998; p 749.
- (91) Robertson, J. Band offsets of wide-band-gap oxides and implications for future electronic devices. *J. Vac. Sci. Technol., B: Microelectron. Process. Phenom.* **2000**, *18*, 1785.
- (92) Mönch, W. Metal–semiconductor contacts: Electronic properties. *Surf. Sci.* **1994**, *299–300*, 928–944.
- (93) Galeener, F. L.; Mikkelsen, J. C.; Geils, R. H.; Mosby, W. J. The relative Raman cross sections of vitreous SiO₂, GeO₂, B₂O₃ and P₂O₅. *Appl. Phys. Lett.* **1978**, *32*, 34.
- (94) Syrotyuk, S.; Shved, V. Electronic excitations in the crystal Li₂O evaluated within Bethe–Salpeter Equation. In *Proceedings of the 2014 IEEE International Conference on Oxide Materials for Electronic Engineering (OMEE 2014)*; IEEE, 2014; p 55.
- (95) Genzel, L.; Martin, T. P. Infrared absorption in small ionic crystal. *Phys. Status Solidi B* **1972**, *51* (b), 91.
- (96) Madelung, O. *Semiconductors: Data Handbook*, 3rd ed.; Springer: Berlin, 2004; pp 187–189.
- (97) Madelung, O. *Semiconductors: Data Handbook*, 3rd ed.; Springer: Berlin, 2004; pp 190–192.
- (98) Feinberg, A.; Perry, C. H. Structural transition and phase transitions in ZrO₂–Y₂O₃ systems. *J. Phys. Chem. Solids* **1981**, *42*, 513–518.
- (99) Madelung, O. *Semiconductors: Data Handbook*, 3rd ed.; Springer: Berlin, 2004; pp 593–594.
- (100) Rebien, M.; Henrion, W.; Hong, M.; Mannaerts, J. P.; Fleischer, M. Optical properties of gallium oxide thin films. *Appl. Phys. Lett.* **2002**, *81*, 250.
- (101) Furthmüller, J.; Bechstedt, J. Quasiparticle bands and spectra of Ga₂O₃ polymorphs. *Phys. Rev. B: Condens. Matter Mater. Phys.* **2016**, *93*, 115204.
- (102) Passlack, M.; Schubert, E. F.; Hobson, W. S.; Hong, M.; Moriya, N.; Chu, S. N. G.; Konstadinidis, K.; Mannaerts, J. P.; Schnoes, M. L.; Zydzik, G. J. Ga₂O₃ films for electronic and optoelectronic applications. *J. Appl. Phys.* **1995**, *77*, 686.
- (103) Lines, M. E. Bond-orbital theory of linear and non-linear electronic response in ionic crystals. I. Linear response. *Phys. Rev. B: Condens. Matter Mater. Phys.* **1990**, *41*, 3372.
- (104) Drablia, S.; Meradji, H.; Ghemid, S.; Boukhris, N.; Bouhafs, B.; Nouet, G. Electronic and optical properties of BaO, BaS, BaSe, BaTe and BaPo compounds under hydrostatic pressure. *Mod. Phys. Lett. B* **2009**, *23*, 3065–3079.
- (105) Hamberg, I.; Granqvist, C. G. Evaporated Sn-doped In₂O₃ films: Basic optical properties and applications to energy efficient windows. *J. Appl. Phys.* **1986**, *60*, R123.
- (106) Ashkenov, N.; Mbenkum, B. N.; Bundesmann, C.; Riede, V.; Lorenz, M.; Spemann, D.; Kaidashev, E. M.; Kasic, A.; Schubert, M.; Grundmann, M.; Wagner, G.; Neumann, H.; Darakchieva, V.; Arwin, H.; Monemar, B. Infrared dielectric functions and phonon modes of high quality ZnO films. *J. Appl. Phys.* **2003**, *93*, 126.
- (107) Hutchins, M.; Abu-Alhair, O.; El-Nahass, M.; El-hady, K. A. Structural and optical characterization of thermally evaporated tungsten trioxide (WO₃) thin films. *Mater. Chem. Phys.* **2006**, *98*, 401–405.
- (108) Gonzalez, R. J.; Zallen, R.; Berger, H. Infrared reflectivity and lattice fundamentals in anatase TiO₂. *Phys. Rev. B: Condens. Matter Mater. Phys.* **1997**, *55*, 7014.
- (109) Dou, M.; Persson, C. Comparative study of rutile and anatase SnO₂ and TiO₂: Band-edge structures, dielectric functions, and polaron effects. *J. Appl. Phys.* **2013**, *113*, No. 083703.
- (110) Davis, T. A.; Vedam, K. Pressure dependence of refractive indices of the tetragonal crystals: KDP, ADP, CaMoO₄, CaWO₄ and rutile. *J. Opt. Soc. Am.* **1968**, *58*, 1446–1451.
- (111) Pang, L.-X.; Zhou, D.; Qi, Z.-M.; Liu, W.-G.; Yue, Z.-X.; Reaney, L. M. Structural-property relationships of sintering temperature scheelite-structured (1-x)BiVO₄–xLaNbO₄ microwave dielectric ceramics. *J. Mater. Chem. C* **2017**, *5*, 2695.
- (112) O’keeffe, M. Infrared optical properties of cuprous oxides. *J. Chem. Phys.* **1963**, *39*, 1789.
- (113) Baumeister, P. W. Optical absorption in cuprous oxide. *Phys. Rev.* **1961**, *121*, 359.
- (114) Garza, A. J.; Scuseria, G. E. Predicting band gaps with hybrid density functionals. *J. Phys. Chem. Lett.* **2016**, *7*, 4165–4170.
- (115) Zheng, H.; Govoni, M.; Galli, G. Dielectric-dependent hybrid functional for heterogeneous materials. *Phys. Rev. Mater.* **2019**, *3*, No. 073803.
- (116) Das, T.; Tosoni, S.; Pacchioni, G. Structural and electronic properties of bulk and ultrathin layers of V₂O₅ and MoO₃. *Comput. Mater. Sci.* **2019**, *163*, 230–240.
- (117) Cassabois, G.; Valvin, P.; Gil, B. Hexagonal boron nitride is an indirect bandgap semiconductor. *Nat. Photonics* **2016**, *10*, 262.
- (118) Bringans, R. D.; Liang, W. Y. Energy bands of the cadmium halides from electron energy loss spectroscopy. *J. Phys. C: Solid State Phys.* **1981**, *14*, 1065.
- (119) Perkins, C. L.; Beall, C.; Reese, M. O.; Barnes, T. M. Two-dimensional cadmium chloride nanosheets in cadmium telluride solar cells. *ACS Appl. Mater. Interfaces* **2017**, *9* (24), 20561–20565.
- (120) Kumari, L.; Li, W. Z.; Vannoy, C. H.; Leblanc, R. M.; Wang, D. Z. Synthesis, characterization, and optical properties of Mg(OH)₂ micro-/nanostructure and its conversion to MgO. *Ceram. Int.* **2009**, *35*, 3355–3364.
- (121) Murakami, T.; Honjo, T.; Kuji, T. DOS calculation analysis of new transparent conductor Mg(OH)₂-C. *Mater. Trans.* **2011**, *52* (8), 1689–1692.
- (122) Al-Gaashani, R.; Radiman, S.; Al-Douri, Y.; Tabet, N.; Daud, A. R. Investigation of the optical properties of Mg(OH)₂ and MgO nanostructures obtained by microwave-assisted method. *J. Alloys Compd.* **2012**, *521*, 71–76.
- (123) Commercial Ca(OH)₂, <https://www.2dsemiconductors.com/caoh2/#description> (accessed June 27, 2019).
- (124) Shibata, T.; Sakai, N.; Fukuda, K.; Ebina, Y.; Sasaki, T. Photocatalytic properties of titania nanostructured films fabricated from titania nanosheets. *Phys. Chem. Chem. Phys.* **2007**, *9*, 2413.
- (125) Greenaway, D. L.; Nitsche, R. Preparation and optical properties of group IV-VI₂ chalcogenides having the CdI₂ structure. *J. Phys. Chem. Solids* **1965**, *26*, 1445–1458.
- (126) Tyagi, P.; Vedeshwar, A. G. Grain size dependent optical band gap of CdI₂ films. *Bull. Mater. Sci.* **2001**, *24* (3), 297–300.
- (127) Gnayem, H.; Sasson, Y. Hierarchical nanostructured 3D flowerlike BiOCl_xBr_{1-x} semiconductors with exceptional visible light photocatalytic activity. *ACS Catal.* **2013**, *3*, 186–191.
- (128) Li, G.; Jiang, B.; Xiao, S.; Lian, Z.; Zhang, D.; Yu, J. C.; Li, H. An efficient dye-sensitized BiOCl photocatalyst for air water purification in visible light irradiation. *Environ. Sci. Process. Impacts.* **2014**, *16*, 1975.
- (129) Bhachu, D. S.; et al. Bismuth oxyhalides: synthesis, structure and photoelectrochemical activity. *Chem. Sci.* **2016**, *7*, 4832.
- (130) Aulich, E.; Brebner, J. L.; Mooser, E. Indirect energy gap in GaSe and GaS. *Phys. Status Solidi B* **1969**, *31*, 129.
- (131) Kenny, N.; Kannewurf, C. R.; Whitmore, D. H. Optical absorption coefficients of vanadium pentoxide single crystals. *J. Phys. Chem. Solids* **1966**, *27*, 1237–1246.
- (132) Meyer, J.; Zilberberg, K.; Riedl, T.; Kahn, A. Electronic structure of Vanadium pentoxide: An efficient hole injector for organic electronic materials. *J. Appl. Phys.* **2011**, *110*, No. 033710.
- (133) Madhuri, K. V.; Naidu, B. S.; Hussain, O. M. Optical absorption studies on (V₂O₅)_{1-x}(MoO₃)_x thin films. *Mater. Chem. Phys.* **2003**, *77*, 22–26.

- (134) Domingo, G.; Itoga, R. S.; Kannewurf, C. R. Fundamental absorption edge in SnS_2 and SnSe_2 . *Phys. Rev.* **1966**, *143* (2), 536.
- (135) Sanchez-Juarez, A.; Ortiz, A. Effects of precursor concentration on the optical and electronic of Sn_xS_y thin films prepared by plasma-enhanced chemical vapour deposition. *Semicond. Sci. Technol.* **2002**, *17*, 931–937.
- (136) Burton, L. A.; Whittles, T. J.; Hesp, D.; Linhart, W. M.; Skelton, J. M.; Hou, B.; Webster, R. F.; O'Dowd, G.; Reece, C.; Cherns, D.; Fermin, D. J.; Veal, T. D.; Dhanak, V. R.; Walsh, A. Electronic and optical properties of single crystal SnS_2 : an earth-abundant disulfide photocatalyst. *J. Mater. Chem. A* **2016**, *4*, 1312.
- (137) Molina-Mendoza, A. J.; et al. Centimeter-scale synthesis of ultrathin layered MoO_3 by van der waals epitaxy. *Chem. Mater.* **2016**, *28*, 4042–4051.
- (138) Shrotriya, V.; Li, G.; Yao, Y.; Chu, C.-W.; Yang, Y. Transition metal oxides as the buffer layer for polymer photovoltaic cells. *Appl. Phys. Lett.* **2006**, *88*, No. 073508.
- (139) Sian, T. S.; Reddy, G. B. Optical, structural and photoelectron spectroscopy studies on amorphous and crystalline molybdenyl oxide thin films. *Sol. Energy Mater. Sol. Cells* **2004**, *82*, 375–386.
- (140) An, H.; Du, Y.; Wang, T.; Wang, C.; Hao, W.; Zhang, J. Photocatalytic properties of BiOX ($X = \text{Cl}, \text{Br}, \text{I}$). *Rare Met.* **2008**, *27* (3), 243.
- (141) Mañas-Valero, S.; García-López, V.; Cantarero, A.; Galbiati, M. Raman spectra of ZrS_2 and ZrSe_2 from bulk to atomically thin layers. *Appl. Sci.* **2016**, *6*, 264.
- (142) Rouibi, L.; Carbone, C. Resonance Raman spectrum of HfS_2 and ZrS_2 . *Phys. Rev. B: Condens. Matter Mater. Phys.* **1988**, *37* (12), 6808.
- (143) Traving, M.; Seydel, T.; Kipp, L.; Skibowski, M.; Starost, F.; Krasovskii, E. E.; Perlov, A.; Schattke, W. Combined photoemission and inverse photoemission study of HfS_2 . *Phys. Rev. B: Condens. Matter Mater. Phys.* **2001**, *63*, No. 035107.
- (144) Gaiser, C.; Zandt, T.; Krapf, A.; Serverin, R.; Janowitz, C.; Manzke, R. Band-gap engineering in $\text{Hf}_{1-x}\text{Se}_{2-x}$. *Phys. Rev. B: Condens. Matter Mater. Phys.* **2004**, *69*, No. 075205.
- (145) Wilson, J. A.; DiSalvo, F. J.; Mahajan, S. Charge-density wave and superlattices in the metallic layered transition metal dichalcogenides. *Adv. Phys.* **1975**, *24* (2), 117–201.
- (146) Marzik, J. V.; Kershaw, R.; Dwight, K.; Wold, A. Photo-electronic properties of ReS_2 and ReSe_2 single crystals. *J. Solid State Chem.* **1984**, *51* (2), 170–175.
- (147) Frey, G. L.; Tenne, R.; Matthews, M. J.; Dresselhaus, M. S.; Dresselhaus, G. Optical properties of MS_2 ($M = \text{Mo}, \text{W}$) inorganic fullerene-like nanotube material optical absorption and resonance Ramon measurement. *J. Mater. Res.* **1998**, *13*, 2412–2417.
- (148) Ogo, Y.; Hiramatsu, H.; Nomura, K.; Yanagi, H.; Kamiya, T.; Hirano, M.; Hosono, H. *p*-channel thin-film transistor using *p*-type oxide semiconductor SnO . *Appl. Phys. Lett.* **2008**, *93*, No. 032113.
- (149) Böker, Th.; Severin, R.; Müller, A.; Janowitz, C.; Manzke, R.; Voß, D.; Krüger, P.; Mazur, A.; Pollmann, J. Band structure of MoS_2 , MoSe_2 , and $\alpha\text{-MoTe}_2$: Angle-resolved photoelectron spectroscopy and *ab initio* calculations. *Phys. Rev. B: Condens. Matter Mater. Phys.* **2001**, *64*, 235305.
- (150) Kam, K. K.; Parkinson, B. A. Detailed photocurrent spectroscopy of the semiconducting group VIB transition metal dichalcogenides. *J. Phys. Chem.* **1982**, *86*, 463–467.
- (151) Zelewski, S.; Kudrawiec, R. Photoacoustic and modulated reflectance studies of indirect and direct band gap in van der Waals crystals. *Sci. Rep.* **2017**, *7*, 15365.
- (152) Eichfeld, S. M.; Eichfeld, C. M.; Lin, Y.-C.; Hossain, L.; Robinson, J. A. Rapid, non-destructive evaluation of ultrathin WSe_2 using spectroscopic ellipsometry. *APL Mater.* **2014**, *2*, No. 092508.
- (153) Yue, R.; Barton, A. D.; Zhu, H.; Azcatl, A.; Pena, L. F.; Wang, J.; Peng, X.; Lu, N.; Cheng, L.; Addou, R.; McDonnell, S.; Colombo, L.; Hsu, J. W. P.; Kim, J.; Kim, M. J.; Wallace, R. M.; Hinkle, C. L. HfSe_2 thin films: 2D transition metal dichalcogenides grown by molecular beam epitaxy. *ACS Nano* **2015**, *9* (1), 474–480.
- (154) Cruz, A.; Mutlu, Z.; Ozkan, M.; Ozkan, C. S. Raman investigation of the air stability of 2H polytype HfSe_2 thin films. *MRS Commun.* **2018**, *8*, 1191–1196.
- (155) Manou, P.; Kalomirov, J. A.; Anagnostopoulos, A. N.; Kambas, K. Optical properties of SnSe_2 single crystal. *Mater. Res. Bull.* **1996**, *31* (11), 1407–1415.
- (156) Mukhokosi, E. P.; Krupanidhi, S. B.; Nanda, K. K. Band gap engineering of hexagonal SnSe_2 nanostructured thin films for intra-red photodetection. *Sci. Rep.* **2017**, *7*, 15215.
- (157) Barry, J. J.; Hughes, H. P.; Klipstein, P. C.; Friend, R. H. Stoichiometric effect in angle-resolved photoemission and transport studies of $\text{Ti}_{1-x}\text{S}_2$. *J. Phys. C: Solid State Phys.* **1983**, *16*, 393–402.
- (158) McElvy, M. J.; Glaunsinger, W. S. Synthesis and characterization of nearly stoichiometric Titanium disulfide. *J. Solid State Chem.* **1987**, *66*, 181–188.
- (159) Singh, A.; Li, Y.; Fodor, B.; Makai, L.; Zhou, J.; Xu, H.; Akey, A.; Li, J.; Jaramillo, R. Near-infrared optical properties and proposed phase-change usefulness of transition metal disulfides. 2019, arXiv:1905.09740 [cond-mat.mes-hall]. arXiv.org e-Print archive. <https://arxiv.org/abs/1905.09740> (accessed June 4, 2019).
- (160) Bayliss, S. C.; Liang, W. Y. Symmetry dependence of optical transitions in group 4B transition metal dichalcogenides. *J. Phys. C: Solid State Phys.* **1982**, *15*, 1283.
- (161) Fischer, D. W. X-ray band spectra and electronic structure of TiS_2 . *Phys. Rev. B* **1973**, *8* (8), 3576.
- (162) Zeppenfeld, K. Electron energy losses and optical anisotropy of MoS_2 single crystals. *Opt. Commun.* **1970**, *1* (8), 377–378.
- (163) Beal, A. R.; Hughes, H. P. Kramers-Kronig analysis of the reflectivity spectra of 2H- MoS_2 , 2H- MoSe_2 and 2H- MoTe_2 . *J. Phys. C: Solid State Phys.* **1979**, *12*, 881.
- (164) Reshak, A. H.; Auluck, S. Band structure and optical response of 2H- MoX_2 compounds ($X = \text{S}, \text{Se}$, and Te). *Phys. Rev. B: Condens. Matter Mater. Phys.* **2005**, *71*, 155114.
- (165) Kumar, A.; Ahluwalia, A. A first-principles comparative study of electronic and optical properties of 1H- MoS_2 and 2H- MoS_2 . *Mater. Chem. Phys.* **2012**, *135*, 755–761.
- (166) Kravets, V. G.; Prorok, V. V.; Poperenko, P. V.; Shaykevich, I. A. Ellipsometry and optical spectroscopy of low dimensional family TMDs. *Fiz. Napirovodn., Kvantova Optoelektron.* **2017**, *20* (3), 284–296.
- (167) Ghosh, C. K.; Sarkar, D.; Mitra, M. K.; Chattopadhyay, K. K. Equibiaxial strain: tunable electronic structure and optical properties of bulk and monolayer of MoSe_2 . *J. Phys. D: Appl. Phys.* **2013**, *46*, 395304.
- (168) Li, Y.; Chernikov, A.; Zhang, X.; Rigosi, A.; Hill, H. M.; van der Zande, A. M.; Chenet, D. A.; Shih, E.-M.; Hone, J.; Heinz, T. F. Measurement of the optical dielectric function of monolayer transition-metal dichalcogenides: MoS_2 , MoSe_2 , WS_2 and WSe_2 . *Phys. Rev. B: Condens. Matter Mater. Phys.* **2014**, *90*, 205422.
- (169) Beal, A. R.; Liang, W. Y. Excitons in 2H- WSe_2 and 3R- WS_2 . *J. Phys. C: Solid State Phys.* **1976**, *9*, 2459.
- (170) Kenny, N.; Kannewurf, C. R.; Whitmore, D. H. Optical absorption coefficients of vanadium pentoxide single crystals. *J. Phys. Chem. Solids* **1966**, *27*, 1237–1246.
- (171) Deb, S. K.; Chopoorian, J. A. Optical properties and color center formation in thin films of molybdenum trioxide. *J. Appl. Phys.* **1966**, *37*, 4818.
- (172) Lucovsky, G.; Mikkelsen, J. C., Jr.; Liang, W. Y.; White, R. M.; Martin, R. M. Optical phonon anisotropies in the layered crystals SnS_2 and SnSe_2 . *Phys. Rev. B* **1976**, *14* (4), 1663.
- (173) Evans, B. L.; Hazelwood, R. A. Optical and electrical properties of SnSe_2 . *J. Phys. D: Appl. Phys.* **1969**, *2*, 1507.
- (174) Allakhverdiev, K. R.; Babaev, S. S.; Salaev, E. Yu.; Tagyev, M. M. Angular behaviour of the polar optical phonons in $\text{Al}^{\text{III}}\text{B}^{\text{VI}}$ layered semiconductors. *Phys. Status Solidi B* **1979**, *96*, 177.
- (175) Segura, A.; Chevy, A. Large increase of the low-frequency dielectric constant of gallium sulfide under hydrostatic pressure. *Phys. Rev. B: Condens. Matter Mater. Phys.* **1994**, *49* (7), 4601.

- (176) Geick, R.; Perry, C. H.; Rupprecht, G. Normal modes in hexagonal boron nitrides. *Phys. Rev.* **1966**, *146*, 543.
- (177) Gavezzotti, A.; Presti, L. Lo. Building blocks of crystal engineering: A large database study of the Intermolecular approach between C-H donor groups and O, N, Cl or F acceptors in organic crystals. *Cryst. Growth Des.* **2016**, *16*, 2952–2962.
- (178) Colombo, V.; Presti, L. Lo.; Gavezzotti, A. Two-component organic crystals without hydrogen bonding: Structure and intermolecular interactions in biomolecular stacking. *CrystEngComm* **2017**, *19*, 2413–2423.
- (179) R Core Team. *R: A Language and Environment for Statistical Computing*; R Foundation for Statistical Computing: Vienna, Austria, 2014; <http://www.R-project.org>.
- (180) Cui, Z.-H.; Wang, Y.-C.; Zhang, M.-Y.; Xu, X.; Jiang, H. Doubly screened hybrid functional: An accurate first-principles approach for both Narrow- and Wide-gap semiconductors. *J. Phys. Chem. Lett.* **2018**, *9*, 2338–2345.